

# Cell Identification and Collection using a Lab-in-a-Fiber Device

Achar. V. Harish<sup>1,2,3†\*</sup>, João C. Varela<sup>2†</sup>, Timothy Gibbon<sup>3</sup>, Walter Margulis<sup>3</sup>, Aman Russom<sup>2</sup>, Fredrik Laurell<sup>1</sup>

<sup>1</sup> Laser Physics, Department of Applied Physics, KTH, Stockholm, Sweden

<sup>2</sup> Division of Nanobiotechnology, Department of Protein Science, Science for Life Laboratory, KTH, Solna, Sweden. <sup>3</sup> Research Institutes of Sweden (RISE), Stockholm, Sweden.

\*E-mail: harishav@kth.se, † These authors contributed equally to this work

We have developed a Lab-in-a-fiber (LIF) module which is capable of selectively detecting and picking up single cells or clusters of labeled cancer cells (MCF-7) for further analysis.

A selective cell picking module was developed from a combination of multimode fiber (MMF) with a core diameter of 62.5  $\mu\text{m}$  and 125  $\mu\text{m}$  cladding diameter and silica capillary with an inner diameter of 90  $\mu\text{m}$  and outer diameter of 125  $\mu\text{m}$ . The MMF identifies cells that were fluorescently labeled by illuminating them with a laser and then collecting the scattered fluorescent light. Once the cell of interest is identified, a pump is activated to gently suck the cell inside the silica capillary. The device has demonstrated the ability to pick single cells as well as clusters of cells. Viability tests conducted on the cells indicate that cells picked up in the silica capillary can be used for further analysis and can be propagated in culture.

The fiber device consists of two uncoated fibers, a multimode fiber used to excite and collect light and a silica fiber capillary with a 90  $\mu\text{m}$  inner diameter and 125  $\mu\text{m}$  outer diameter, used to collect the cells. The two fibers were inserted inside a 260/330  $\mu\text{m}$  housing capillary to obtain a robust unit. The housing capillary was then flooded with sodium silicate (2.5 mol%) water and air-cured to secure the fibers in the desired position. The tip of the fiber component was diced flush using a high-speed rotational diamond blade and then treated with a hydrophobic liquid to secure the fibers.

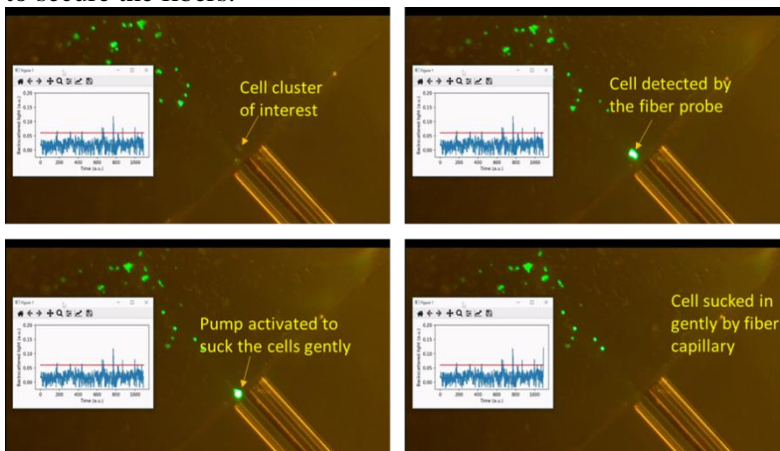


*Fig. 1* Snapshots of the fluorescent cell cluster being captured by our optical fiber probe. The pump gently sucks in the cells and can be further used for analysis and cell culture.

A 488 nm laser was used to excite calcein-AM labeled cells, and the fiber device was mounted on a 3D-translation stage to be swept throughout the sample using a joystick with a precision of nearly 1  $\mu\text{m}$ . When a labeled cell was illuminated, a fluorescent signal was collected by the MMF, separated by a dichroic mirror, and detected with a photomultiplier unit (PMT). When the signal was above a preset threshold, a negative pressure of approximately 1 bar was applied with a vacuum pump to the capillary, and the cell was captured. The successful collection of cells from tumor spheroids and small tumor pieces shows the potential of this component to be implemented in a clinical setting, especially for in vivo diagnosis of

hard-to-treat cancers, where sample collection is particularly difficult.

This fiber-based cell-picking device can be combined with other technologies for quick downstream analysis, alongside another capillary, allowing for local, precise point-of-care

## References

- [1] Hu, P., Zhang, W., Xin, H., & Deng, G. (2016). *Frontiers in Cell and Developmental Biology*, 4, 2296-634X.
- [2] Keiser, G., Xiong, F., Cui, Y., & Shum, P. P. (2014). *Journal of Biomedical Optics*, 19(8).
- [3] Harish, A. V., Kumar, T., Etcheverry, S., Margulis, W., Laurell, F., & Russom, A. (2023). *Lab Chip*, 23, 2286-2293.

# A draw-tower fabricated optical fiber for distributed H2 sensing

Sandy Alomari<sup>1,2</sup>, Kenny Hey Tow<sup>1</sup>, Joao Pereira<sup>1</sup>, Ari Antikainen<sup>1</sup>, Tedros Weldehawariat<sup>1</sup>, Korina Hartmann<sup>3</sup>, Remco Nieuwland<sup>3</sup>, Åsa Claesson<sup>1</sup>

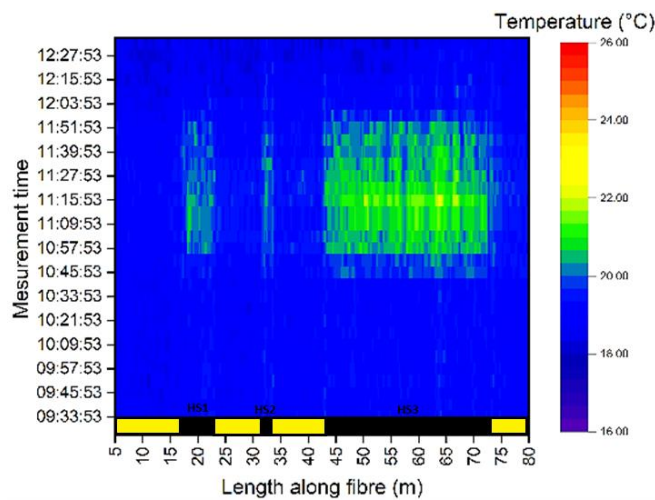
1. RISE Research Institutes of Sweden, Fiberlab, Fibervägen 2, 824 50 Hudiksvall, Sweden
2. Royal Institute of Technology, Roslagstullsbacken 21, 114 21 Stockholm, Sweden
3. United Fiber Sensing B.V., Spui 37, 2511 BL, The Hague, The Netherlands

Hydrogen is gaining importance as a clean energy carrier, but its safe handling is critical. Leaks must be detected early to prevent accidents and to reduce the loss of hydrogen, which is also an indirect greenhouse gas.

We present the development and demonstration of a distributed hydrogen leak detection sensor, with the potential to monitor large areas of infrastructure, in a safe and reliable fiber optic setup.

A distributed hydrogen sensor was developed where an optical fiber was coated with a hydrogen sensitive material. The material heats up in the presence of hydrogen due to an exothermal reaction between the gas and the active coating. The temperature increase can then be probed with conventional fiber optic distributed temperature sensor systems (DTS).

The sensing concept was evaluated in a hydrogen facility at RISE using an off-the-shelf Raman DTS, where the fiber was mounted inside an autoclave and subjected to 4 vol% of hydrogen in air.



DTS measurement of the fiber under test versus time, showing the evolution of the temperature at three different hotspots during the experiment.

## References:

S. Alomari, K. Hey Tow, J. Pereira, A. Antikainen, T. Weldehawariat, K. Hartmann, R. Nieuwland, and Å. Claesson. "Distributed Hydrogen Sensing and Leak Detection Using Draw-Tower Fabricated Optical Fiber," OPTICA advanced photonic congress 2024, doi: 10.1364/SOF.2024.SoTh1F.2

# Establishing a Quantum Communication Link Over 200 km of Deployed Optical Fiber

Joakim Argillander<sup>1†</sup>, Martin Clason<sup>1</sup>, and Guilherme B. Xavier<sup>1</sup>

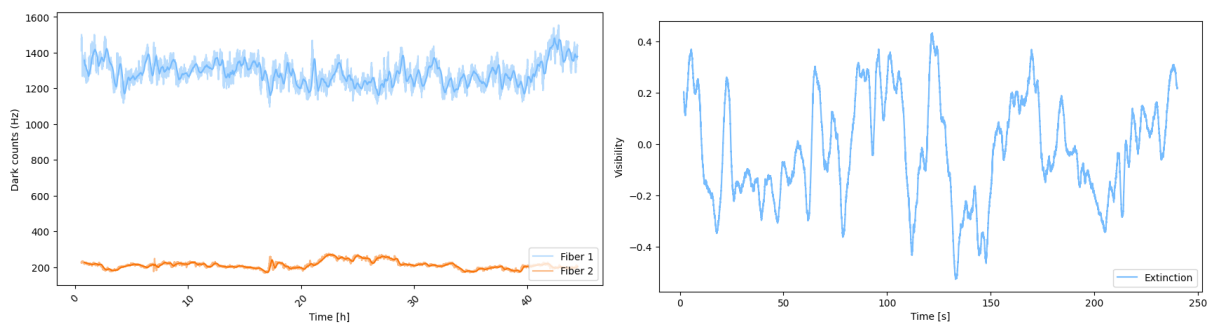
<sup>1</sup>Department of Electrical Engineering, Linköping University, SE-581 83 Linköping, Sweden

October 15, 2024

Sweden being a sparsely populated country with comparatively long distances between cities poses a challenge for the establishment of a quantum communication link between larger cities. Conventional quantum communication links are typically done over shorter distances between buildings or adjacent cities. [1] In particular, as part of the European Council's Quantum Communication Infrastructure (QCI) initiative, the establishment of a quantum communication link between Linköping and Stockholm in Sweden is of interest. In this study we measure a suite of parameters that are relevant for the establishment of a quantum communication link over 200 km of deployed optical fiber. We measure the attenuation, single-photon background count rate and polarization drift of the fiber using a superconducting nanowire single-photon detector (SNSPD). As can be seen in fig. 1a, the background photon count rate in the link remains stable over the course of 42 hours.

We further characterize the link interferometrically by implementing a Sagnac interferometer with the entire link constituting the loop. We measure the visibility of the interferometer as a function of time over 42 hours. The use of Sagnac interferometers as foundation for quantum key distribution (QKD) is proposed to eliminate differential phase noise between the two arms of the interferometer [2]. However, we experience a significant drift in the visibility of the interferometer over time as shown in fig. 1b. The reason for this drift is currently unknown and is subject to further investigation.

This study marks a significant step towards the establishment of a quantum communication link in Sweden between Linköping and Stockholm, and this serves as a reference for future quantum communication links over long distances.



(a) Dark count of the 200km link over time

(b) Visibility over time of the Sagnac interferometer

## References

1. Chung, J. *et al.* *Quantum Information Science, Sensing, and Computation XIII* **11726** (SPIE, 2021), 1172602.
2. Qi, B., Huang, L.-l., Lo, H.-k. & Qian, L. *2006 IEEE International Symposium on Information Theory* (2006), 2090–2093.

**Enkeleda Balliu, PhD**

**Senior Laser Engineer and Product Manager**



**Cobolt AB, a part of HÜBNER Photonics**

### **Abstract**

Quantum technologies are evolving rapidly, driving an increasing demand for the enabling technologies that support them. Among these, laser systems play a pivotal role in the precise control and manipulation of quantum systems. Applications such as atom trapping & cooling as well as quantum state manipulation for quantum computer processes require lasers with exceptional stability, spectral purity, tunability, and low noise to ensure coherence and accuracy in delicate quantum environments. This study explores how advanced laser systems—including tunable continuous-wave sources, ultra-low-noise fiber amplifiers, and high-power stable lasers—meet the stringent demands of these quantum applications.

High spectral purity and stability are critical for ensuring accuracy in quantum sensing and interferometry, where even minimal frequency drift can disrupt measurements. Lasers with narrow linewidths and stable output power allow for consistent and precise manipulation of quantum states. Furthermore, ultra-low-noise amplification is essential for maintaining the coherence of quantum systems, reducing noise that could otherwise compromise experiments. This is particularly crucial in applications sensitive to external perturbations, such as atom trapping and cooling.

The ability to tune continuous-wave lasers across a wide range of wavelengths provides precise control over atomic transitions, optimizing interactions in complex quantum setups. Combined with high-power sources that maintain stability under demanding conditions, these laser systems deliver robust performance across a wide range of quantum experiments, from trapping and cooling of atoms to precision measurements and quantum computing.

This work demonstrates how the performance characteristics of these advanced laser systems collectively enhance the precision, stability, and scalability of quantum applications. Their contribution to new breakthroughs in quantum research underlines their importance as essential tools in the next generation of quantum platforms.

# Backward Wave Optical Parametric Oscillator Targeting CO<sub>2</sub> Absorption Lines at 2.7 $\mu$ m

Adrian Vågberg<sup>1,†,\*</sup>, Martin Brunzell<sup>1,†</sup>, Max Widarsson<sup>2</sup>, Patrick Mutter<sup>1,2</sup>, Andrius Zukauskas<sup>1</sup>, Fredrik Laurell<sup>1</sup>, Valdas Pasiskevicius<sup>1</sup>

<sup>1</sup>Department of Applied Physics, KTH Royal Institute of Technology, Roslagstullsbacken 21, 106 91 Stockholm, Sweden

<sup>2</sup>SLF Svenska Laserfabriken AB, Ruddammsvägen 49, 114 19 Stockholm, Sweden

<sup>†</sup>The authors contributed equally to this work

\*avag@kth.se

**Abstract:** The first demonstration of a 2.7  $\mu$ m CO<sub>2</sub> gas sensing source exploiting a *backward wave optical parametric oscillator* (BWOPO). Transmission measurements of the backward wave are demonstrated through air with good agreement with simulations.

Increasing the precision of existing climate models requires higher spatial resolution concentration data for the most ubiquitous greenhouse gases, CO<sub>2</sub> and water vapour being two of them [1]. Active sensing systems based on differential absorption LIDARs deployed in low Earth orbit satellites offer a promising avenue for high resolution and wide coverage. Such missions require environmentally robust light sources with high spectral stability, a possibility for fine-tuning of the wavelength, and narrow spectral bandwidth for precisely targeting vibrational-rotational molecular lines [2,3]. A *backward wave optical parametric oscillator* (BWOPO) potentially offers the required characteristics [4]. In a BWOPO, the oscillation is established due to the counterpropagating parametric interaction without the need for optical cavities. This process also ensures high wavelength stability and narrow bandwidth of the backward-generated wave.

In this work, we present, to the best of our knowledge, the first BWOPO precisely tuning over several CO<sub>2</sub> absorption lines, demonstrating the viability of this simple narrowband parametric light source. Moreover, the counterpropagating nonlinear interaction ensures narrowband backward wave generation even when pumped with a multi-longitudinal mode laser with an unstable mode spectrum. The BWOPO is realized in periodically poled KTiOPO<sub>4</sub> (PPKTP) with submicron poling periodicity. The periodicity was chosen for the generation of the backward idler wave at 2.712  $\mu$ m when pumping at 1.03  $\mu$ m. This idler wavelength region was selected to coincide with relatively strong CO<sub>2</sub> (and H<sub>2</sub>O vapor ) absorption lines, allowing for direct CO<sub>2</sub> spectral measurements in the ambient laboratory air.

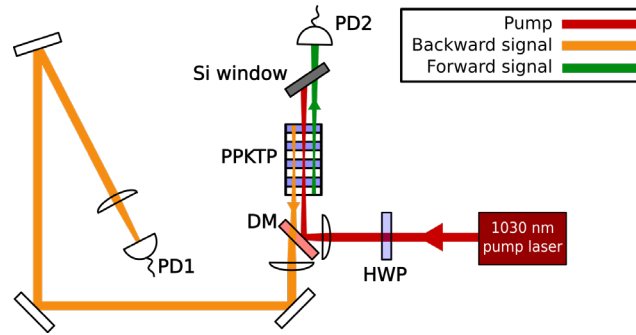


**Figure 1:** Schematic of the experimental setup for the BWOPO CO<sub>2</sub> gas absorption measurements. The pump operates at 1030 nm, the backward signal is centered around 2712 nm and forward signal at 1661 nm.

Figure 1 illustrates the experimental setup where the pump laser (Thorlabs QSL103A, 380 ps, 9 kHz) generating pulses with a maximum energy of 45  $\mu$ J is guided into the PPKTP. The pump laser was multi-longitudinal mode with a spectral width of 360 GHz.

Tuning the backward wave output was performed by changing the PPKTP temperature (see Figure 2 (a)). Experimentally, the tuning was measured with an optical spectrum analyzer and calibrated by observing the absorption dips at one H<sub>2</sub>O and two CO<sub>2</sub> rovibrational lines. The positions of these lines are well known from the

HITRAN database [5]. Tuning rates are compared to those obtained from Sellmeier equations [6]. The results are highly consistent with each other giving the temperature tuning rate of 1.77 GHz/K. The absorption line scan (see Figure 2 (b)) was measured by tracking powers of the forward and backward waves simultaneously. Due to Manley-Rowe's condition, the ratio of the powers will be constant unless one of the waves suffers excess losses in the air. This measurement protocol reduces the influence of the pump power fluctuations. Using this procedure a transmission measurement through  $\sim 290$  cm of ambient air was captured as the PPKTP temperature was tuned (see Figure 2 (b)). The data overlaps well with the HITRAN simulations, where the oscillations at the long-wavelength end and the small discrepancy at short wavelengths are attributed to the detection scheme. The  $2.7 \mu\text{m}$  backward wave was captured on a detector with a rise-time in the order of seconds while the forward wave could be captured on a significantly faster detector ( $<1 \mu\text{s}$  rise time). This asymmetry falsely correlated fast noise as long-term trends, distorting the results slightly. The strong decrease in the transmission at wavelengths shorter than  $2.712 \mu\text{m}$  is due to an adjacent  $\text{H}_2\text{O}$  absorption line.

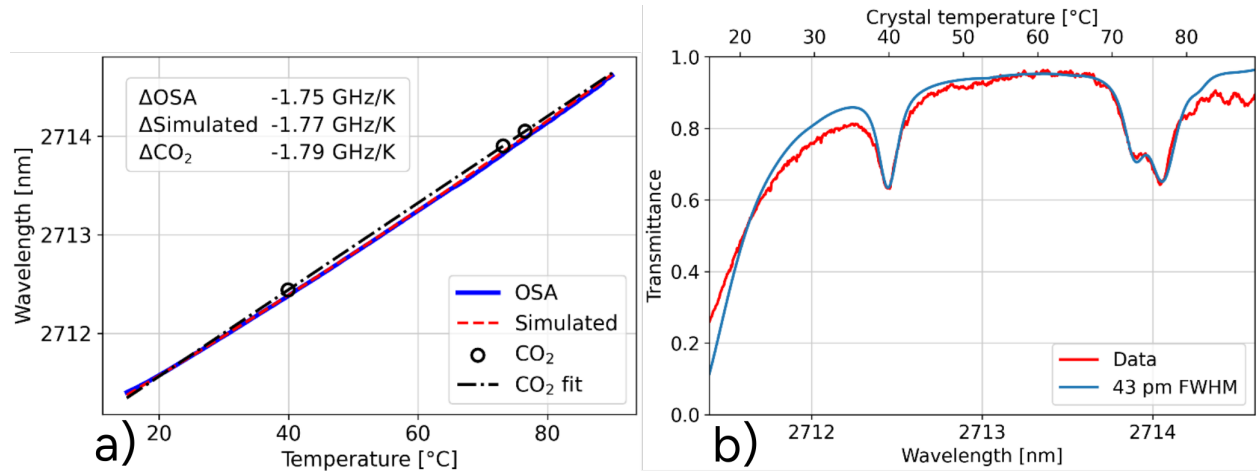


**Figure 2:** Measurements from the BWOPO system is illustrated. (a) the tuning with respect to crystal temperature is presented and compared to Sellmeier equations and by measuring the location of the three distinct  $\text{CO}_2$  dips. The  $\text{CO}_2$  fit is a straight line going through the absorption peaks. (b) The transmission spectrum of the ambient air in the lab is shown and compared with a HITRAN-simulated trace.

The bandwidth of the backward wave was too narrow for the OSA to properly capture its true width. Another approach was chosen where the convolution of the simulated trace and Gaussian-like spectrum of varying widths was compared to the measured trace. By choosing the width of the Gaussian to minimize the error, an estimate of the backward linewidth was measured to be approximately 43 pm ( $\sim 1.7$  GHz).

Further studies of the wavelength stability using the transmission spectra are presented. The intensity noise is measured at two regions: one where the transmission has locally no dependence on wavelength and the other where the local dependence is maximized. The resulting noise difference gives an upper limit on center wavelength stability of 65 MHz; however, it is very likely that the system exhibits a significantly higher stability.

In conclusion, this work demonstrates that a simple BWOPO, even pumped with a multimode laser is perfectly suitable for  $\text{CO}_2$  gas sensing. The technology can readily target suitable absorption lines for a given application. For instance, for a space-borne system, weaker absorption lines at wavelengths within the PPKTP transmission band can be chosen.

## References

- [1] Z. Wang and M. Menenti, "Challenges and Opportunities in Lidar Remote Sensing," *Frontiers in Remote Sensing* 2, (2021).
- [2] F. Gibert, D. Edouard, C. Cénac, F. Le Mounier, and A. Dumas, "2- $\mu\text{m}$  Ho emitter-based coherent DIAL for  $\text{CO}_2$  profiling in the atmosphere," *Opt Lett* 40, 3093 (2015).
- [3] Y. Liu, K. M. Mølster, A. Zukauskas, C. S. J. Lee, and V. Pasiskevicius, "Type-II PPRKTP optical parametric oscillators in the 2  $\mu\text{m}$  spectral range," *J. Opt. Soc. Am. B* 40, A36-A43 (2023)
- [4] K. M. Mølster, M. Guionie, P. Mutter, J.-B. Dherbecourt, J.-M. Melkonian, X. Délen, A. Zukauskas, F. Laurell, P. Georges, M. Raybaut, S. Godard, and V. Pasiskevicius, "Highly-efficient, high average power, narrowband pump-tunable BWOPO" *Opt. Lett.*, 48, 6484 (2023)
- [5] R. V. Kochanov, I. E. Gordon, L. S. Rothman, P. Weislo, C. Hill, and J.S. Wilzewski, "HITRAN Application Programming Interface (HAPI): A comprehensive approach to working with spectroscopic data," *J Quant Spectrosc Radiat Transf* 177, 15 (2016).
- [6] M. Katz, D. Eger, M. B. Oron, and A. Hardy, "Erratum: "Refractive dispersion curve measurement of  $\text{KTiOPO}_4$  using periodically segmented waveguides and periodically poled crystals" [*J. Appl. Phys.* 90, 53 (2001)]," *J Appl Phys* 92, 7702 (2002)

# Distributed fibre-Optic Acoustic Sensing – A new tool for geophysical surveys

Kenny Hey Tow<sup>a</sup>, Åsa Claesson<sup>a</sup>, Joao Pereira<sup>a</sup>, Miguel Soriano-Amat<sup>a</sup>, Matteo Rossi<sup>b</sup>

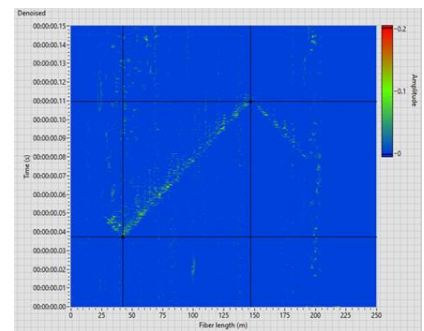
<sup>a</sup>RISE Research Institutes of Sweden, Fiber Optics and Photonics Unit, Sweden.

<sup>b</sup>Engineering Geology Division, Lund University, Sweden

## ABSTRACT

Distributed acoustic Sensing (DAS) is an advanced fibre-optic sensing technology that converts a standard telecom fiber into a linear array of microphones, which can pick up vibrations every few meters over tens of kilometers. These sensors also come with all the intrinsic advantages linked to optical fibers: no electrical power is required along the optical fiber beyond the interrogator, small size, immunity to electromagnetic interference and corrosion, and the capability to survey up to several kilometers using a single optical fiber cable, exceeding the maximum length of hydrophone cables. Hence, a DAS-based solution leads to logistically easier and more accurate seismic characterizations, resulting in less time consuming and more cost-effective geophysical campaigns.

Over the past few years, RISE Fibre Optics has been working towards developing customised DAS interrogator systems in different application areas, including seismic measurements during geophysical surveys. In this communication, the feasibility of associating this advanced sensing technique with standard telecom optical fibres for measuring vibration data as a complement to traditional seismic acquisitions during geophysical surveys will be presented for two use cases: (i) monitoring mining induced seismicity during mine exploitation and (ii) investigating bedrock quality at the bottom of water bodies. Event detection such as production blasts and small seismic activities could be detected in a tunnel during mine exploitation as well as seismic waves propagating at the bottom of a lake (see figure as example). Future work will be oriented towards using these types of measurements to provide useful information about the elastic properties of the rock and the relative local response to man-induced seismic events.



## ACKNOWLEDGEMENTS

The authors would like to acknowledge Impakt AB, LKAB and Stiftelsen Bergteknisk Forskning for their support.

---

\*Further author information: send correspondence to Kenny Hey Tow (kenny.heytow@ri.se)

# Self Monitoring Quantum Random Number Generator using Photonic Shot Noise

Martin Clason<sup>1†</sup>, Joakim Argillander<sup>1</sup>, and Guilherme B. Xavier<sup>1</sup>

<sup>1</sup>Department of Electrical Engineering, Linköping University, SE-581 83 Linköping, Sweden

October 15, 2024

Random numbers play a crucial role in various scientific and technological applications like simulations and secure communication. In most cases both the uniformity and the unpredictability of the generated bits are crucial. One approach to generating unpredictable random numbers is by sampling noise and using this data as the entropy source for the generator. The discretization of light into photons, a quantum phenomenon, gives rise to shot noise which can be amplified and digitized [1]. If a random number generator can sample noise from a system and demonstrate that a significant proportion of the noise originates from photonic shot noise, it would indicate the quantum nature of the sampled noise. By estimating the electron charge from the sampled noise, we are able to assess the quality of the noise source while simultaneously generating random bits from the same data. We use an operational amplifier in a transimpedance configuration to amplify noise from a photodiode illuminated by an LED. By selecting the optimal feedback resistance (which corresponds to the amplifier gain) we minimize thermal noise in the system and achieve an estimate of the electron charge with a relative error of 3%.

This work paves the way for cheaper QRNGs with built-in self monitoring as a pragmatic compromise to more secure schemes like device independent random number generators [2].

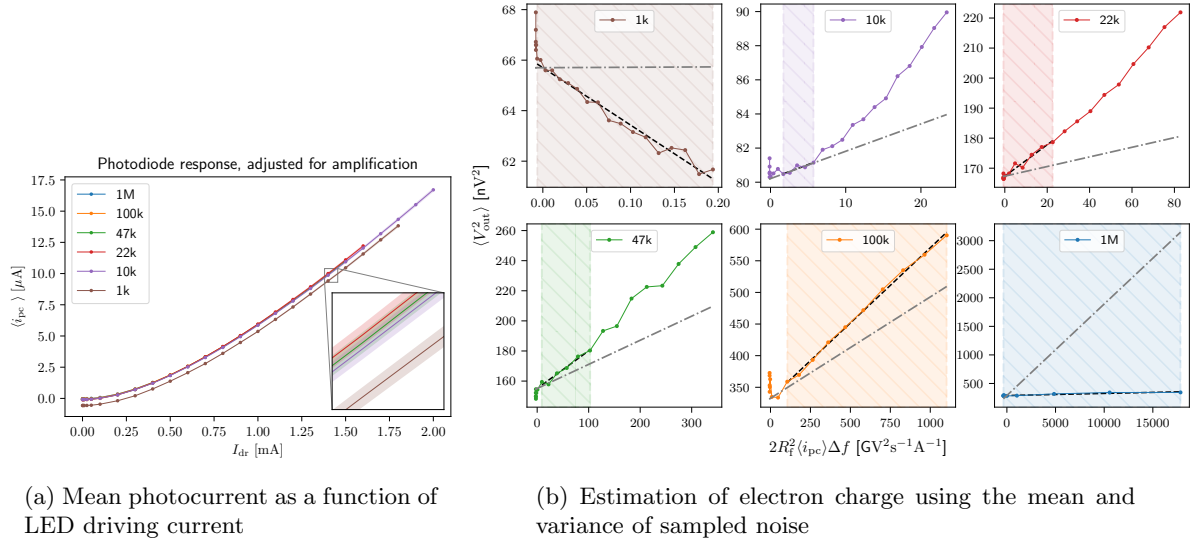


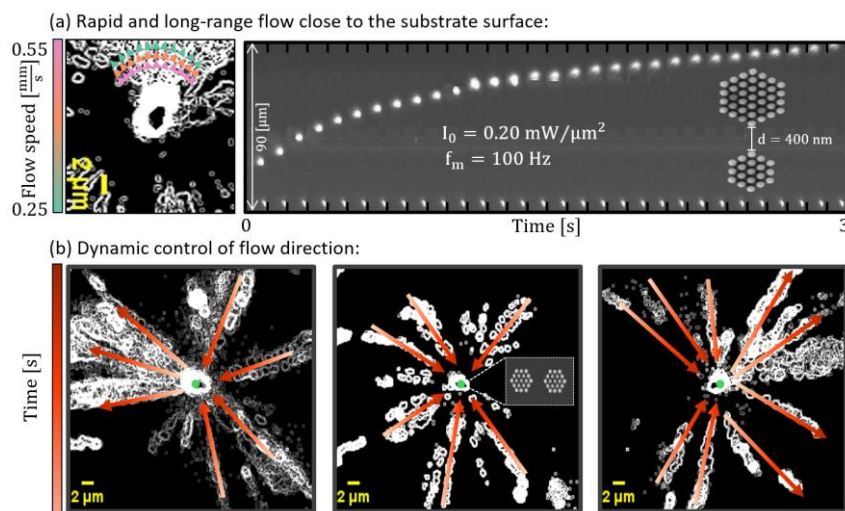
Figure 1: Obtained data for feedback resistances ranging from 1 k $\Omega$  to 1 M $\Omega$

## References

1. Fox, M. *Quantum optics: an introduction* (Oxford Univ. Press, Oxford, 2006).
2. Herrero-Collantes, M. & Garcia-Escartin, J. C. Quantum random number generators. en. *Reviews of Modern Physics* **89**, 015004 (2017).

## Directional Marangoni flow induced by laser heating of amorphous silicon nanodisks

**Abstract:** Gold nanostructures are often used for optical heating, but they can be unstable and prone to melting under prolonged light exposure and high temperatures [1, 2]. To address these challenges, this study investigates the use of amorphous silicon (a-Si) nanodisks as a more stable and biocompatible alternative for photothermal applications. a-Si, known for its higher melting threshold and thermal stability, offers promising performance as a nanoheater. Our results demonstrate that a-Si nanodisks can efficiently vaporize water to generate microbubbles under continuous-wave (CW) laser illumination. These microbubbles induce strong, localized fluid flows, governed by the Marangoni effect, where temperature gradients along the bubble surface create surface tension differences that induce the flow [3]. We observed that these flows are capable of rapid transportation of microparticles over significant distances (Figure 1a), and their direction can be controlled by adjusting the laser position (Figure 1b).



(a) Marangoni flow generated by asymmetric pairs of a-Si nanodisk arrays, consisting of 37 and 19 nanodisks. *Left panel:* The velocity and trajectories of 1  $\mu\text{m}$  diameter polystyrene (PS) beads moving around the arrays due to bubble-induced flow. *Right panel:* Video stills showing a 2 mm probe at the liquid interface being pushed away by the flow generated from the nanodisk pair. The nanodisks appear as two bright white dots at the bottom of the image. The inset shows an SEM micrograph of the nanodisk pair. (b) Marangoni flow produced by symmetric a-Si nanodisk arrays, each containing 19 nanodisks. The velocity and trajectories of 1  $\mu\text{m}$  PS beads are shown for three laser focus positions: *Left panel:* Laser focused on the left array; *Middle panel:* Laser focused on the center of the gap between the two arrays; *Right panel:* Laser focused on the right array. The inset in the middle panel provides an SEM micrograph of one of the arrays.

### References:

1. Hu, M. , et al., Investigation of the properties of gold nanoparticles in aqueous solution at extremely high lattice temperatures. *Chemical physics letters*, 2004. **391**(4-6): p. 220-225.
2. Plech, A., et al., Laser-induced heating and melting of gold nanoparticles studied by time-resolved x-ray scattering. *Physical Review B—Condensed Matter and Materials Physics*, 2004. **70**(19): p. 195423.
3. Baroud, C.N., Thermocapillarity, in *Encyclopedia of Microfluidics and Nanofluidics*, D. Li, Editor. 2013, Springer US: Boston, MA. p. 1-7.

# Laser-Enhanced Nanoporous Graphite Anodes for Next-Generation Lithium-Ion Batteries

Luke Bond, Henrik Andersson, Magnus Hummelgård and Magnus Engholm\*

Dept. Of Engineering, Mathematics and Science Education, Mid Sweden University, Sundsvall

Lithium-ion batteries are central to advancing energy storage technologies, with graphite anodes being a key component due to their high theoretical capacity and reliable cycle life[1]. However, the performance of graphite anodes is often limited by lithium-ion storage capacity [2] and ion diffusion rates [3]. To address these challenges, modifications at the nanoscale, such as increasing porosity [4] and altering the spacing between graphite layers [5], have been explored. Our research introduces an innovative, industrially scalable laser processing technique that transforms a low-cost nano-graphite and graphene mixture into a nanoporous structure, enabling significant improvements in battery performance. This one-step laser method not only optimizes surface morphology but also enhances lithium-ion diffusion and intercalation. The laser-processed anodes exhibit substantially improved specific capacities across all charge rates, particularly excelling at higher rates. In long-term cycling tests at 1C, these anodes demonstrated superior durability and performance, achieving specific capacities of 323 mAh/g compared to 241 mAh/g for untreated samples. This work showcases the potential of laser-driven material modifications in advancing LIB technology and highlights the broader applicability of such approaches in enhancing energy storage solutions.

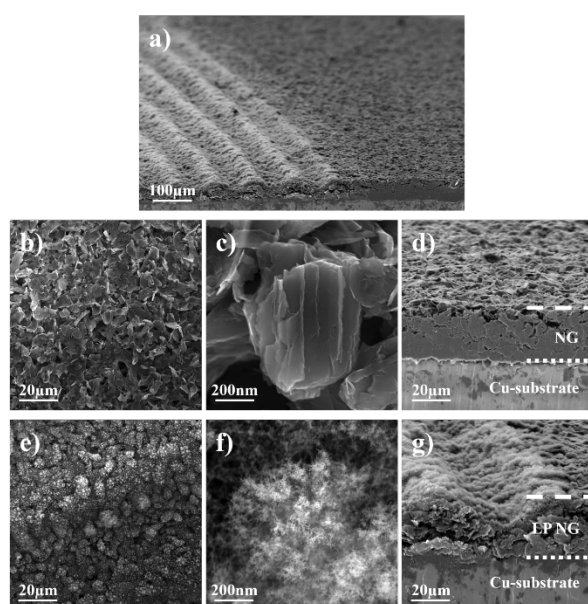


Figure 1 SEM images of a) cross-section of NG and laser-processed NG surfaces, NG b,c) surface, and d) cross-section, laser processed NG e,f) surface, and g) cross-section. The Cu substrate and coatings are labelled, with edges marked.

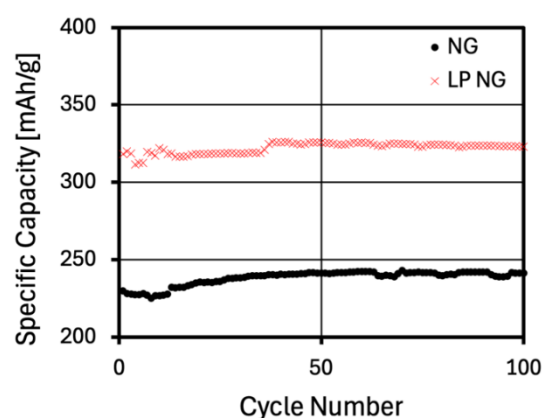


Figure 2 Mean average galvanostatic charge-discharge cycling of NG (black solid circles) and laser-processed NG (red crosses) cell sets at a 1C charge rate.

- [1] M. Phadatare *et al.*, 'Silicon-Nanographite Aerogel-Based Anodes for High Performance Lithium Ion Batteries', *Sci Rep*, vol. 9, no. 1, Art. no. 1, Oct. 2019, doi: 10.1038/s41598-019-51087-y.
- [2] D. Jang *et al.*, 'Enhancing rate capability of graphite anodes for lithium-ion batteries by pore-structuring', *Applied Surface Science Advances*, vol. 6, p. 100168, Dec. 2021, doi: 10.1016/j.apsadv.2021.100168.
- [3] D.-K. Son, J. Kim, M. R. Raj, and G. Lee, 'Elucidating the structural redox behaviors of nanostructured expanded graphite anodes toward fast-charging and high-performance lithium-ion batteries', *Carbon*, vol. 175, pp. 187–201, Apr. 2021, doi: 10.1016/j.carbon.2021.01.015.
- [4] O. Mypati *et al.*, 'The synthesis of novel porous graphene anodes for fast charging and improved electrochemical performance for lithium-ion batteries', *Energy Sources, Part A: Recovery, Utilization, and Environmental Effects*, vol. 44, no. 2, pp. 4349–4363, Jun. 2022, doi: 10.1080/15567036.2022.2075990.
- [5] Y. Lee, S. M. N. Jeghan, and G. Lee, 'Boost charging lithium-ion battery using expanded graphite anode with enhanced performance', *Materials Letters*, vol. 299, p. 130077, Sep. 2021, doi: 10.1016/j.matlet.2021.130077.

# Synthesis of Yb:YVO<sub>4</sub> Nanoparticles via Femtosecond Laser Ablation in Liquid

Luke Bond, Ellinor Jönsson and Magnus Engholm\*

Dept. of Engineering, Mathematics and Science Education, Mid Sweden University, Sundsvall

Nanoparticles are increasingly used in various applications from healthcare [1] to energy storage [2]. Pulsed laser ablation in liquid (PLAL) has emerged as a promising technique for nanoparticle production, offering advantages like high purity and precise size control [3]. Although traditionally hindered by low production rates, recent advancements in laser scanning technology, such as polygon scanners, have enabled production rates of grams per hour [4], positioning PLAL as a more industrially scalable technique. In photonics, rare-earth doped nanoparticles like Yb:YVO<sub>4</sub> are particularly interesting due to their favorable thermal properties and potential applications in laser-active materials [5]. Here, we present an investigation of the synthesis of Yb:YVO<sub>4</sub> nanoparticles using a 1030 nm femtosecond laser, focusing on how parameters such as pulse repetition rate and solvent composition influence nanoparticle size and morphology. We observed ovoid-like structures in deionized water and spherical particles with enhanced colloidal stability in ammonia, with particle sizes ranging from 10 to 150 nm. Notably, the structural integrity of the nanoparticles, including their composition and crystalline features, remains consistent with that of the bulk Yb:YVO<sub>4</sub> target material after processing. Characterization was carried out using dynamic light scattering, Raman spectroscopy, scanning electron microscopy, and energy-dispersive X-ray spectroscopy. These findings demonstrate the potential of femtosecond laser ablation to produce high-quality nanoparticles, paving the way for future advancements in scalable nanoparticle production for photonic applications.

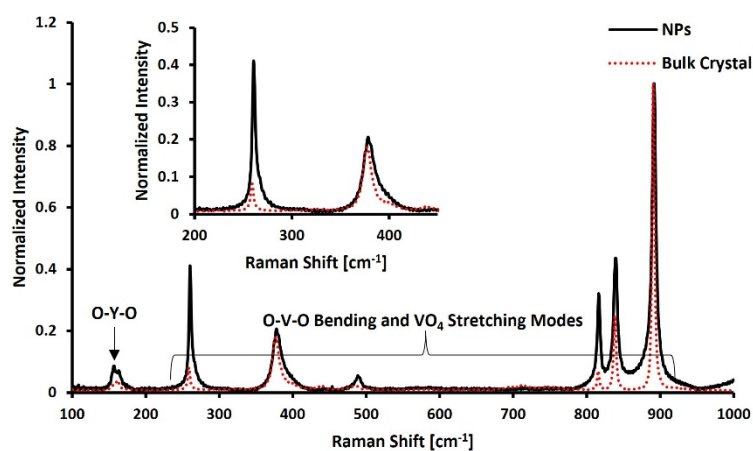
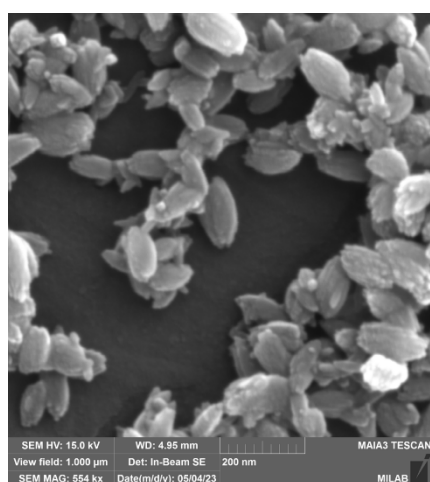


Figure 1 Typical SEM imaging of NPs synthesized via PLAL, using DI water. indicating standard ovoid-like NPs, synthesized using 0.1 kHz pulse repetition rate for 30 minutes

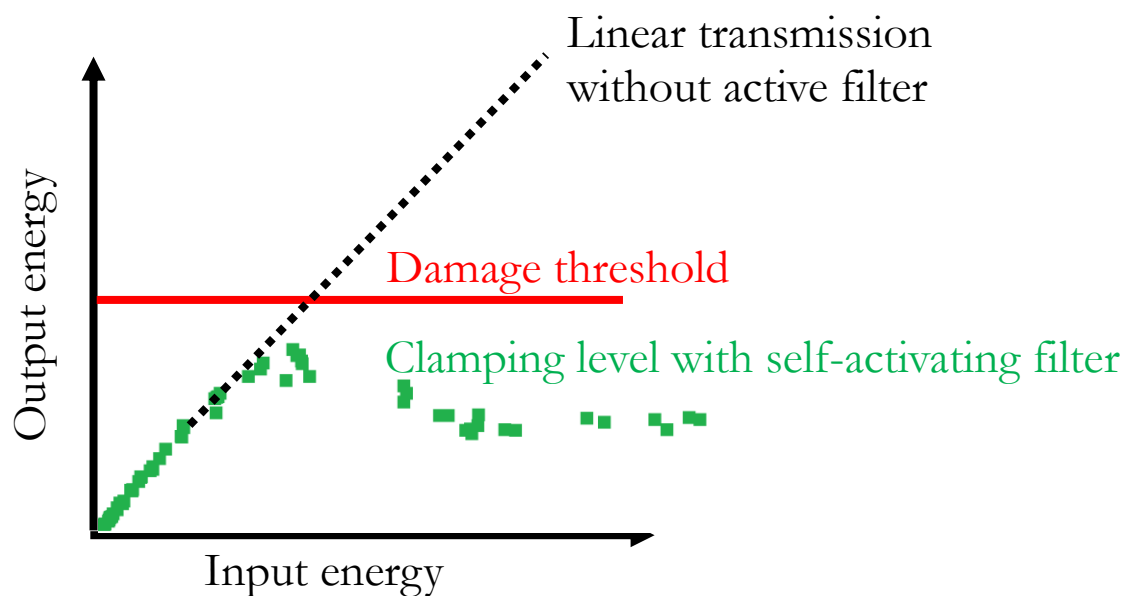
Figure 2 Raman spectra of bulk Yb:YVO<sub>4</sub> crystal (blue), compared to typical spectra of NPs synthesized in DI water (red).

- [1] K. Cho, X. Wang, S. Nie, Z. (Georgia) Chen, and D. M. Shin, 'Therapeutic Nanoparticles for Drug Delivery in Cancer', *Clinical Cancer Research*, vol. 14, no. 5, pp. 1310–1316, Mar. 2008, doi: 10.1158/1078-0432.CCR-07-1441.
- [2] Y. Gogotsi and R. M. Penner, 'Energy Storage in Nanomaterials – Capacitive, Pseudocapacitive, or Battery-like?', *ACS Nano*, vol. 12, no. 3, pp. 2081–2083, Mar. 2018, doi: 10.1021/acsnano.8b01914.
- [3] M. Kim, S. Osone, T. Kim, H. Higashi, and T. Seto, 'Synthesis of Nanoparticles by Laser Ablation: A Review', *KONA*, vol. 34, pp. 80–90, 2017, doi: 10.14356/kona.2017009.
- [4] R. Streubel, S. Barcikowski, and B. Gökce, 'Continuous multigram nanoparticle synthesis by high-power, high-repetition-rate ultrafast laser ablation in liquids', *Opt. Lett.*, *OL*, vol. 41, no. 7, pp. 1486–1489, Apr. 2016, doi: 10.1364/OL.41.001486.
- [5] N. Stopikowska, M. Runowski, P. Woźny, S. Lis, and P. Du, 'Generation of Pure Green Up-Conversion Luminescence in Er<sup>3+</sup> Doped and Yb<sup>3+</sup>-Er<sup>3+</sup> Co-Doped YVO<sub>4</sub> Nanomaterials under 785 and 975 nm Excitation', *Nanomaterials*, vol. 12, no. 5, Art. no. 5, Jan. 2022, doi: 10.3390/nano12050799.

# Self-activating filter for optical power limiting (OPL)

Rikard Forsén, Cesar Lopes and Nils Ross, FOI Swedish Defence Research Agency  
Carole Vaillant, Stephane Parola, Denis Chateau, et al., ENS Lyon

Inspired by sol-gel materials<sup>1</sup> we have developed a transparent and colorless SiO<sub>2</sub>-based low temperature melting gel<sup>2,3</sup>. The gel is a 3D-polymer network of SiO<sub>2</sub> with phenyl groups impeding condensation into SiO<sub>2</sub>. It is cheap to synthesize through a sol-gel process at around 100 °C. The concentration ratio of two precursors, phenyltriethoxysilane (PhTES) and diphenyldiethoxysilan (DPhDES), determines the melting properties of the gel. In our case, we have tuned the gel to transfers from an elastic to a viscous phase at 80 °C. This allows for doping with sensitive organic molecules with nonlinear absorption. The gel exhibits an optical power limiting effect, which self-activates thermally by intense hazardous light. The gel shows self-healing properties and it is re-shapeable after synthesis. The gel is suitable as a self-activating filter inside optical systems to protect sensors, an eye or skin.



<sup>1</sup> L. C. Klein, et al., J. Sol-Gel Sci. Technol. 2010, 55(1), 86

<sup>2</sup> Nils Ross, M.Sc. thesis 87424, 2021, FOI and Luleå University

<sup>3</sup> Work in manuscript.

# Generation of circular THz vortex by direct optical rectification

Yaqun Liu, Valdas Pasiskevicius

Department of Applied Physics, Royal Institute of Technology, Albanovägen 29, 114 19 Stockholm, Sweden

Author e-mail address: [yaqun@kth.se](mailto:yaqun@kth.se)

**Abstract:** A circularly-polarized THz vortex was generated using field synthesis in optical rectification of two interfering near-infrared delayed vortices. Two-dimensional electro-optic imaging and terahertz polarimetry techniques were employed for frequency-resolved THz field amplitude and phase characterization.

Terahertz (THz) attracts great interest for its existing and potential applications in spectroscopy, imaging, sensing, and communication [1-3]. Circularly polarized vortex THz beams, which contain both orbital angular momentum (OAM) and spin angular momentum (SAM), provide additional tools for applications in the next generation of wireless communications, spectroscopy, and manipulation of novel magnetic and chiral materials, and others [4, 5]. Here, we propose an experimental method to directly generate a circularly polarized vortex THz beam by OR using two vortex infrared femtosecond beams with an adjustable phase difference.

The setup for the generation of the THz vortex beam is shown in Fig. 1(a). A linearly polarized laser with a central wavelength of 800 nm, a pulse duration of 33 fs, and a repetition rate of 1 kHz was used as pump and probe. The two pump beams are 45° polarized with each other with the balanced power. A delay line controlled the pulse delay between two pump beams. An S-waveplate was inserted to convert linear polarized pumps into radially polarized beams with the polarization winding number of 1 before [111]-cut ZnTe. The probe beam was used for 2D time-resolved EO imaging in a [110]-cut ZnTe crystal. Two wire-grid polarizers were inserted before the EO crystal for THz field polarimetry.

To generate a THz vector vortex beam with a helicity, a non-zero time-delay was introduced between two pump vortices. The characteristics of circular THz vortex at 1 THz were illustrated in Fig. 1(b), and the results were observed from the point of source. The phases and amplitudes distribution with the first THz wire-grid polarizer along X and Y axis (see Fig. 1(a)) are depicted in Fig. 1 (b)-i, ii, iv and v. The phase profiles both exhibit a clockwise of  $4\pi$  indicating the presence of OAM of  $+2\hbar$ . The theoretical state of polarization of this circular vortex is depicted in Fig. 1(b)-iii. The typical electric-field trajectory of the generated THz waveform was shown in Fig. 1(b)-vi. The helicity was verified as right-handed, suggesting a SAM of  $+\hbar$ . The total angular momentum of this circular polarized terahertz vortex summed up to  $+3\hbar$ .

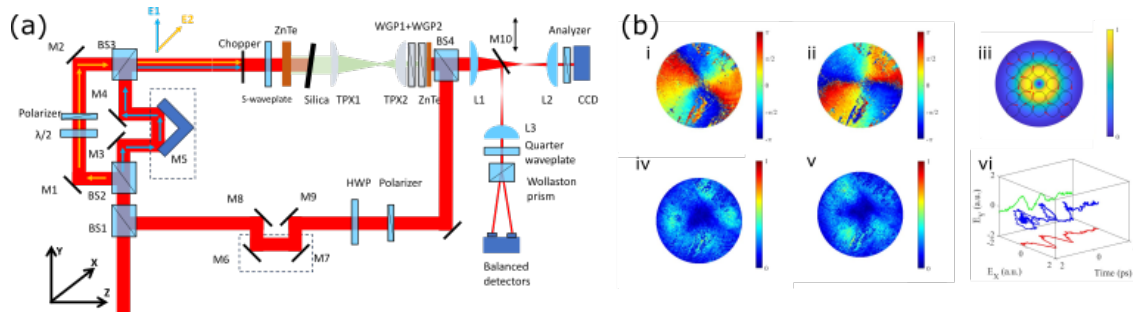


Fig. 1. The schematic diagram of THz generation and imaging setup (a). BS1-4: beam splitters. HWP: half waveplate. M1-M10: reflective mirrors. L1-L3: focusing lenses. TPX1, TPX2: TPX lens, WGP1, WGP2 wire grid THz polarizers. E1, E2: polarization of two pumps. Dashed frames: delay lines. Left corner: XYZ laboratory coordinate system. Measurement of the circular THz vortex (b). (i) Transverse phase distribution of X axis polarized, and (ii) Transverse phase distribution of Y axis polarized THz field. (iii) Transverse amplitude distribution of X axis polarized, and (iv) Transverse amplitude distribution of Y axis polarized THz field. Color bars in (i) and (ii) show the phase scale (radian), and color bars in (iii) and (v) represent the field amplitudes in arbitrary units. (v) State of polarization profile. (vi) Electric field trajectory of THz waveform.

In conclusion, we proposed and experimentally demonstrated an approach to generate the circularly polarized terahertz vortex field using OR of two infrared vortices. The total angular momentum and chirality, and frequency-resolved characteristics of circular THz vortex were studied by 2D THz-TDS and polarimetry technique. This approach provides the potential to synthesize more complex vector THz beams, broadening the possible THz applications.

## References

- [1] Tonouchi, M. Nature Photon 1, 97–105 (2007).
- [2] F. Hindle, R. Bocquet, A. Pienkina, A. Cuisset, and G. Mouret, Optica 6 (2019).
- [3] Nagatsuma, T., Ducournau, G. & Renaud, C. Nature Photon 10, 371–379 (2016).
- [4] Minagawa, H., Yoshimura, S., Terasaka, K. et al. Sci Rep 13, 15400 (2023).
- [5] Jepsen, P. U., Cooke, D. G. & Koch, M. Laser Photon Rev. 5,124–166 (2011).

## D-scan: basic principles

**Author:** Marzo López Cerón (cr0676lo-s@student.lu.se) (Master Student)

**Co-authors:** Daniel Díaz Rivas, Ivan Sytceвич, Ann-Kathrin Raab, Miguel Canhota, Chen Guo, Anne L’Huillier and Cord Arnold

The dispersion scan (d-scan) is a technique aimed for ultrafast pulse characterisation in the femtosecond regime. The technique is based on generating a non-linear signal from the pulse to be measured while manipulating its spectral phase. The manipulation of the phase is done by introducing different amounts of group delay dispersion (GDD) to the beam. In this case, the second harmonic is generated, and the outcome is a two-dimensional trace of the SH spectrum vs. the introduced dispersion. This trace allows a numerical retrieval of the spectral phase, which ultimately permits the temporal profile and phase to be obtained [1], [2], [3].

Two approaches of this technique are presented: the scanning d-scan and the single-shot (s-shot) d-scan.

The scanning d-scan uses translating wedges in order to introduce different amounts of dispersion to the beam, which then is directed to a BBO crystal where the second harmonic is generated. Afterwards it reaches a spectrometer that records the signal. This approach allows the measurement of few- and many-cycle femtosecond pulses [2].

Due to its scanning nature, the d-scan only provides averaged measurements, which is totally fine as long the laser source is stable. For low repetition rate ultrafast lasers, however scanning can take inconveniently long and single-shot pulse characterisation is preferable. Furthermore, single-shot approaches can give immediate feedback to the laser operator. The s-shot is a single-shot d-scan implementation, introducing different amounts of GDD to different spatial parts of the beam using material dispersion. A prism of a dispersive material, suitable for the time regime and wavelength of the pulse to be measured is placed before the BBO to achieve spatially varying dispersion. Once again, the generated second-order non-linear signal is recorded with a spectrometer, and the pulse can be retrieved with the same mathematical methods [1].

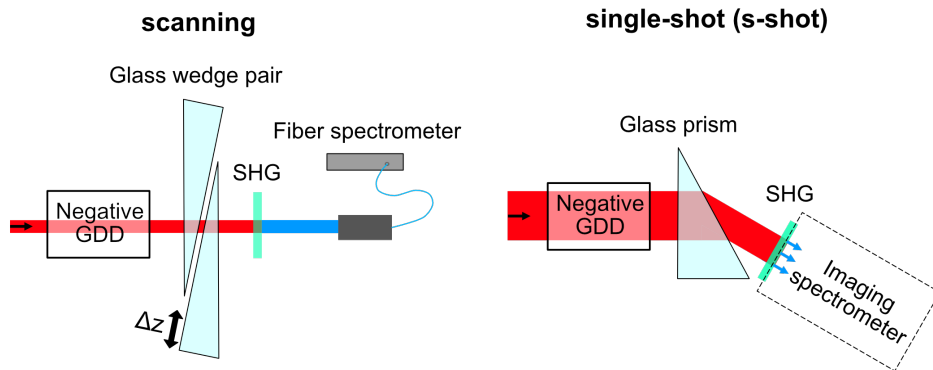


Figure 1: Scanning d-scan and single-shot d-scan basic set-up

## References

- [1] Maïté Louisy et al. “Compact single-shot d-scan setup for the characterization of few-cycle laser pulses”. en. In: *Applied Optics* 56.32 (Nov. 2017), p. 9084.
- [2] Miguel Miranda et al. “Simultaneous compression and characterization of ultrashort laser pulses using chirped mirrors and glass wedges”. en. In: *Optics Express* 20.1 (Jan. 2012), p. 688.
- [3] Ivan Sytceвич et al. “Characterizing ultrashort laser pulses with second harmonic dispersion scans”. en. In: *Journal of the Optical Society of America B* 38.5 (May 2021), p. 1546.

# Revealing the Fano Combs in Mie Scattering

Javier Tello Marmolejo, Adriana Canales, Dag Hanstorp, and Ricardo Méndez-Fragoso

Presenter: Javier Tello Marmolejo

A droplet trapped in an optical trap emits light in complex patterns called Mie Scattering. The scattering includes Transverse Electric (TE) and Magnetic (TM) modes in all directions and polarizations, resulting in a pattern full of overlapping resonances. Although the problem has an analytical solution, the full spectrum is so complex that recognizable patterns have not been found and is only understood by comparing to numerical simulations. Here we show the arising structure of Fano combs in the directional Mie scattering of evaporating water droplets [1]. It shows how resonances arrange themselves in consecutive combs. Inside of each comb the Q-factor of the resonances rises exponentially, resulting in extreme sensitive to absorbance at the far right of the combs. The spectrum is fully defined by the refractive index of the droplet, allowing us to measure the refractance and absorbance in absolute terms, for a spectrum of wavelengths. In other words, a refractometer and spectrophotometer in one, with detection limit in absorbance from  $10^{-3}$  to  $10^{-8}$  and a precision of about 10%.

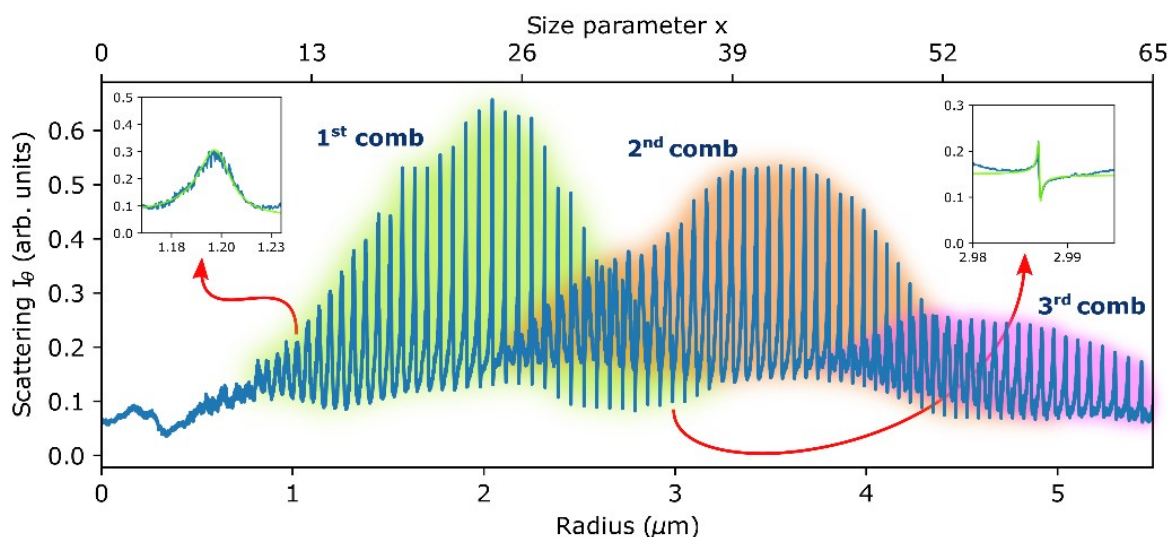


Fig. 1 The size dependent resonances of a sphere arrange themselves in combs made up of evolving Fano profiles from broad and symmetric to narrow and asymmetric.

[1] *Fano Combs in the Directional Mie Scattering of a Water Droplet*, Javier Tello Marmolejo, Adriana Canales, Dag Hanstorp, and Ricardo Méndez-Fragoso, *Phys. Rev. Lett.* **130**, 043804, (2023)

## Optical simulator of a double potential well in quantum mechanics

R. Méndez-Fragoso<sup>1</sup>, V. Zuñiga-Perez<sup>2</sup>, and D. Hanstorp<sup>3</sup>

<sup>1</sup>Facultad de Ciencias, Universidad Nacional Autónoma de México, México.

<sup>2</sup>Faculty of Engineering, Friedrich-Alexander University, Germany.

<sup>3</sup>Physics Department, University of Gothenburg, Sweden.

We build a double optical tweezer that generates two potential wells capable of trapping micrometric particles. When these are very close, a double optical potential well is produced. We use a piezoelectric dispenser to deposit silicone oil particles with sizes between 20 and 35  $\mu\text{m}$ . In the experiment we can control the relative intensity between each of the wells and the distance that separates them in order to take advantage of the Brownian motion of the particle and thus produce spontaneous jumps between them [1]. We use a lens array and two perpendicular Position Sensing Detectors to locate the particle in three dimensions along its trajectory. With this information we make statistics of the particle's movement over time to show that this system is analogous to a particle in a double potential well used in quantum mechanics [2]. Properties that both systems share are calculated for different parameters of the experiment. This contribution is one of the first steps towards future experiments in which properties of atomic systems can be simulated using analogues in optics.

[1] Loïc Rondin, Jan Gieseler, Francesco Ricci, Romain Quidant, Christoph Dellago, and Lukas Novotny. Direct measurement of kramers turnover with a levitated nanoparticle. *Nature Nanotechnology*, 12:1130–1133, 2017.

[2] Yu P. Kalmykov, W. T. Coffey, and S. V. Titov. On the brownian motion in a double-well potential in the overdamped limit. *Physica A: Statistical Mechanics and its Applications*, 377:412–420, 4 2007.

## Metrology for wearable light loggers and optical radiation dosimeters

Nilsson Tengelin, M<sup>1</sup>, Källberg, S.<sup>1</sup>, Svensson, I.<sup>1</sup>

<sup>1</sup> Department of Measurement Science and Technology, RISE Research Institutes of Sweden, Borås, SWEDEN

Maria.Nilssontengelin@ri.se

### Abstract

Light exposure significantly affects human health and behaviour, modulating sleep, cognitive functions and neuroendocrine processes. The effects of light on human physiology can be observed acutely as changes in subjective alertness, mood, sleep architecture, heart rate and suppression of the hormone melatonin, usually produced by the brain before the biological night. The invention of electric lighting has led people to spending more time indoors during the day, including working remotely from home, and staying up later in the evening. However, the intensity of artificial light is only a fraction of that of daylight (a half for a cloudy sky, and less than 1 % of a sunny afternoon), while their spectral compositions differ in terms of blue light proportion. Implications for health and well-being vary from mood and wakefulness to sleep deprivation, including severe health problems, such as depression and heart diseases.

New standardised metrics for measuring the physiological, non-visual effects of light have been recently introduced and wearable light loggers have been developed as a way to measure an individual's personal light dose. However, the optical characterisation of these dosimeters is challenging because of the compromises needed to make them wearable and affordable. This poster presents the work performed in the European project "Metrology for wearable light loggers and optical radiation dosimeters – MeLiDos", which aims to provide the scientific and industrial communities with the necessary tools (e.g. best practice guides) for the characterisation and use of wearable light loggers and solar UV dosimeters.

In this project characterisation methods for wearable optical radiation dosimeters are under development and will in the next step be validated in an international intercomparison. Five different wearable light loggers from different manufacturers in different price ranges have been acquired. Also, three different solar UV-dosimeters from different manufacturers are being characterized and compared.

Further analysing the quality of data collection methods, a multi-center field study with wearable light loggers is being performed where research subjects in six different countries (Sweden, Germany, The Netherlands, Spain, Turkey and Ghana) are wearing light loggers for one week while also reporting sleep quality, mood and tiredness.

**Keywords:** Wearable light logger, light dosimeter, non-image forming effects, UV-dosimeter

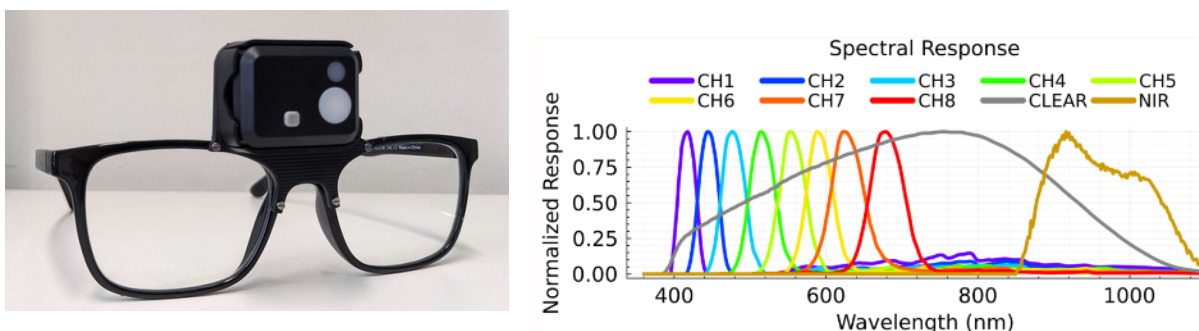


**Figure 1 – The wearable light logger used in the multi-centric field study (left). The spectral response of the different channels of the light logger (right).**

## Sound, Light and Design in the Intensive Care Unit: SoLiDe-ICU 2030

Nilsson Tengelin, M<sup>1</sup>, Olausson, S.<sup>2,3</sup>, Johansson, L.<sup>2,3</sup>, Sundberg, F.<sup>4,5</sup>, James, F.<sup>6</sup>

<sup>1</sup> Department of Measurement Science and Technology, RISE Research Institutes of Sweden, Borås, Sweden

<sup>2</sup> Institute of Health and Care Sciences, Sahlgrenska Academy, University of Gothenburg, Gothenburg, Sweden

<sup>3</sup> Sahlgrenska University Hospital, Department of Anaesthesiology and Intensive Care, Gothenburg, Sweden

<sup>4</sup> Research and Development Centre, Skaraborg Hospital Skövde, Region Västra Götaland, Skövde, Sweden

<sup>5</sup> The School of Health Sciences, University of Skövde, Skövde, Sweden

<sup>6</sup> Academy for Design and Crafts, University of Gothenburg, Gothenburg, Sweden

Maria.Nilssontengelin@ri.se

### Abstract

This poster describes a multidisciplinary research project that aims to generate knowledge and improve the physical environment and its impact on staff's health and wellbeing in intensive care units (ICUs). ICUs are complicated hospital units to design due to the complex nature of the clinical care and the needs of patients, families, and staff. The growing amount of technology has led to cramped spaces causing difficulties to perform nursing and medical interventions. Workers in these environments face a significant probability of experiencing physical and psychological symptoms associated with environmental discomfort which may also affect the patient care. Despite advances in critical care, the physical environment continues to be an area that calls for improvement. More knowledge is needed concerning environmental factors like sound, light and spatial layout.

Visual discomfort can negatively affect the ability to perform different tasks; too high or too low light levels may lead to headache, eyestrain or fatigue. Light plays a crucial role in regulating wakefulness and alertness and limited access to 'daylight-like' light during the day may result in fatigue and depression, and too much light at night-time with frequently occurring high intensity interruptions may lead to sleep disturbances. Furthermore, alarm and monitoring sounds can cause psychological stress for both patients and staff, and intermittent, uncontrollable sounds can induce acute stress reactions. Noise in the workplace can impair communication ability with the patients, concentration and attention, and lead to fatigue.

In this project, the light and sound exposures of members of the staff in the ICU at Sahlgrenska University Hospital are to be measured both with wearable devices and by characterization of the lighting and acoustics in the different rooms of the workplace. The impact of light and noise on the staff's mood, alertness wellbeing and sleep during the study period is estimated using questionnaires. Environmental factors causing interruptions leading to missed nursing care and stress among ICU staff is identified by including observational protocols, self-reported stress questionnaires, and physiological stress indicators like heart rate variability (HRV) and skin conductance.



Figure 1 – Work environment in the ICU

# On-Chip Lasers on Waveguides

A Meta-Morphosis in Waveguide Imaging!

Oliver Olsson,<sup>1</sup> Khosro Zangeneh Kamali,<sup>1</sup> Erik Strandberg,<sup>2</sup> Hana Šípová-Jungová<sup>1</sup> and Mikael Käll.<sup>1</sup>

<sup>1</sup>Department of Physics, Chalmers University of Technology, 412 96, Gothenburg, Sweden

<sup>2</sup>Department of Microtechnology and Nanoscience, Chalmers University of Technology, 412 96 Gothenburg, Sweden

Scattering-based microscopy methods has recently gathered attention as an alternative to the ubiquitous fluorescence microscopy [1] with several configurations showing super-resolution by techniques such as structured illumination [2] or coherent light [3]. The advantages of scattering over fluorescence include: 1) no requirement for fluorescent tagging of the imaged object - scattering microscopy is *label-free*; 2) experiment times is not limited, fluorescent tags get photobleached; 3) scattering does not get saturated, the fluorophore do, which limits the rate of detection [4].

To suppress the background signal and only collect the scattered light, darkfield imaging (DF) or total internal reflection (TIR) are frequently used where TIR generates an *evanescent field* which generates scattering from the object. Another efficient way to achieve evanescent fields is to couple the excitation light to a waveguide. Multiple configurations have been realized using materials such as silicon dioxide and a polymer [5], microscope slides [6], or silicon nitride [7]. However, the current platforms utilize external lasers that couples the light into the waveguide by *butt-coupling*. This makes the platform complex to use and more sensitive to outer disturbances.

By integrating a laser directly onto a waveguide, a fully on-chip illumination source can be fabricated. This illumination source would not require any additional equipment and would generate a scattering TIR illumination platform for a standard microscope.

Vertical cavity surface emitting lasers (VCSELs) were recently used for label-free imaging in both darkfield and TIR. This was made possible by deflecting the light with a monolithically integrated metasurface, deflecting the beam at a high angle [8]. We are now expanding this concept by coupling the VCSELs light into a waveguide, thereby providing more uniform illumination with ultralow background and an expanded field-of-view.

1. Astratov, V.N., et al., *Roadmap on Label-Free Super-Resolution Imaging*. Laser & Photonics Reviews, 2023. **17**(12): p. 2200029.
2. Heintzmann, R. and T. Huser, *Super-Resolution Structured Illumination Microscopy*. Chemical Reviews, 2017. **117**(23): p. 13890-13908.
3. Jünger, F., P.V. Olshausen, and A. Rohrbach, *Fast, label-free super-resolution live-cell imaging using rotating coherent scattering (ROCS) microscopy*. Scientific Reports, 2016. **6**(1): p. 30393.
4. Priest, L., J.S. Peters, and P. Kukura, *Scattering-based Light Microscopy: From Metal Nanoparticles to Single Proteins*. Chemical Reviews, 2021. **121**(19): p. 11937-11970.
5. Agnarsson, B., et al., *Evanescence Light-Scattering Microscopy for Label-Free Interfacial Imaging: From Single Sub-100 nm Vesicles to Live Cells*. ACS Nano, 2015. **9**(12): p. 11849-11862.
6. Yang, S., et al., *Waveguide-based microscope slide for label-free high-resolution imaging*. Applied Physics Letters, 2024. **125**(6).
7. Helle, Ø.I., et al., *Structured illumination microscopy using a photonic chip*. Nature Photonics, 2020. **14**(7): p. 431-438.
8. Juodėnas, M., et al., *High-angle deflection of metagrating-integrated laser emission for high-contrast microscopy*. Light: Science & Applications, 2023. **12**(1).

# Measuring the phase of a dark pulse

Christoffer Oxelmark Krook<sup>†</sup>, Martin Brunzell<sup>†</sup>, Fredrik Laurell and Valdas Pasiskevicius

<sup>†</sup> Authors contributed equally

Department of Applied Physics, Royal Institute of Technology, Albanovägen 29, 114 29 Stockholm, Sweden

Dark pulses are pulses characterised by a temporal dip in the intensity. Examples of applications for such pulses are optical gyroscopes and telecommunication links [1, 2]. Their reduced sensitivity to transmission losses and lower intensity, and thus reduced sensitivity to nonlinear effects, means that they propagate differently to normal pulses. After their theorisation, experimental verification has so far mostly been the generation of optical dark solitons in optical fibres. Recent publications have demonstrated free-space propagating dark pulses on the picosecond timescale, synchronized to partnered bright pulses [3]. To measure the intensity of dark pulses is easily achievable by means of photodetectors, the phase however remains inherently different to characterise because of the relatively low intensity.

In this article we demonstrate for the first time ever experimental characterisation of the phase of a dark pulse which is achieved by means of blind-FROG measurements in combination with a new FROG algorithm with a reduced sensitivity to measurement noise [4, 5].

The dark pulses are generated through intra-cavity sum-frequency generation between two lasers, resulting in synchronised bright and dark pulses. These bright and dark pulses have comparable bandwidths to each other which makes them suitable candidates for a blind cross-correlation measurement. The experimental set-up can be seen in fig. 2 and the results can be observed in fig. 2 and demonstrates a discrete near- $\pi$  phase-jump in the temporal phase profile, as is expected in simulations. Further, the intensity profile shows bumps along the sides of the dark pulse, matching what is to be expected during bright-dark pulse pair generation under group-velocity mismatch [6].

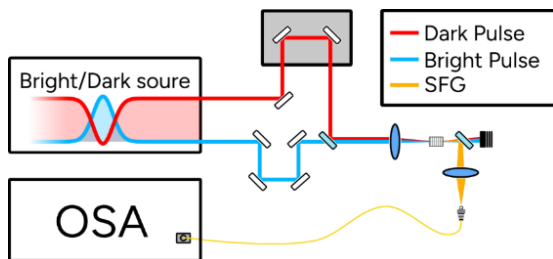


Figure 2: Experimental set-up for the blind FROG measurement

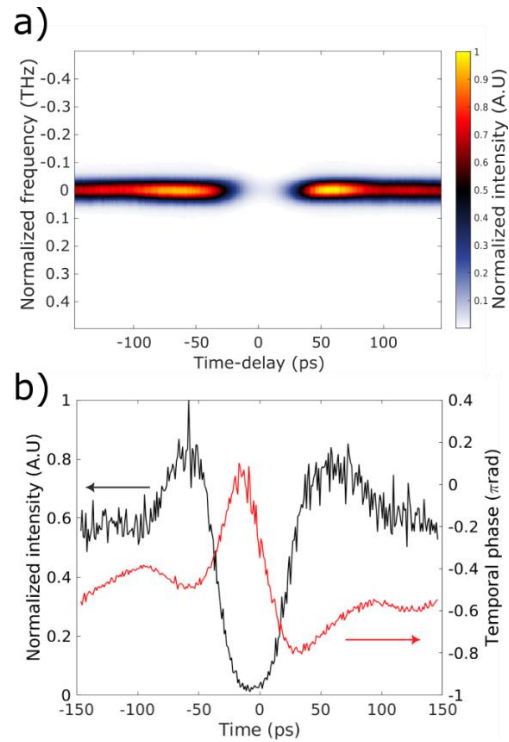


Figure 1. a) Measured blind-FROG trace b) Retrieved dark pulse intensity and phase.

## References

- 1: Rene-Jean Essiambre and Govind P Agrawal, *PROGRESS IN OPTICS: SOLITON COMMUNICATION SYSTEMS*, 37th ed. (Elsevier, 1997).
- 2: L. C. B. Silva and C. E. S. Castellani, "Recent progress in optical dark pulses generation based on saturable absorber materials," *Optical Fiber Technology* **64**, (2021).
- 3: M. Widarsson, M. Brunzell, F. Laurell, and V. Pasiskevicius, "Self-mode-locking through intra-cavity sum-frequency generation," *Opt Express* **30**, 40906 (2022).
- 4: R. Trebino, "Measuring Two Pulses Simultaneously: Blind FROG," in *Frequency-Resolved Optical Gating: The Measurement of Ultrashort Laser Pulses*, R. Trebino, ed. (Springer, 2000), pp. 345–355.
- 5: C. Krook, K. Claessen, and V. Pasiskevicius, "Line-search FROG algorithm for retrieval of pulses from noisy datasets," *EPJ Web Conf.* **267**, (2022).
- 6: Shuangyou Zhang, et al, "Dark-Bright Soliton Bound States in a Microresonator", *Phys. Rev. Lett.* **128**, 2022.

# High-Precision Bone Microtomy Using Femtosecond Lasers: Impact of Flat-Top Beam Shaping

Aswin Prakash A<sup>1,2</sup>, Lu Di<sup>1</sup>, Dag Hanstorp<sup>1</sup>

<sup>1</sup>-Department of Physics, University of Gothenburg, SE-412 96 Gothenburg, Sweden

<sup>2</sup>-International School of Photonics, Cochin University of Science and Technology, Kochi 682022, India

## ABSTRACT

Laser Microtomy utilizing Femtosecond lasers presents a cutting-edge method for non-contact sectioning of biological tissues or materials with high precision and minimum thermal damage. Laser microtome can handle hard materials, including bones, teeth, and ceramics. They can slice tissues with minimal damage, which is crucial for immunohistology investigations.

In this study, we focus on optimizing laser beam parameters for sectioning mouse femur bones, which demands high precision. Generally, laser pulses with a Gaussian profile result in a non-uniform intensity distribution, causing tapering along the edges and compromising the quality of the sectioning's surface. To ensure a uniform intensity profile across the sample, we can employ flat-top beams to provide consistent cuts.

For the femtosecond laser bone sectioning of mouse femur bones, a CPA-2001 Amplified kHz Ti: Sapphire Laser System (Clark-MXR, Inc) operating at a wavelength of 775 nm, alongside beam shaping optics, a high-power objective lens, and a motorized sample position system is used to manipulate the cutting process. The femtosecond laser creates sectioning with low thermal shocked zones, which is beneficial for the preservation of tissues.

The aim is to produce thin slices of bones nearly 10 micrometers thick while preserving the cellular integrity. Presently, we are working on beam-shaping optics to achieve the desired flat-top profile and to focus the beam to femur bone using high objective lens while maintaining its profile, which can minimize the edge effects while enhancing the uniformity of the intensity profile. The cutting process is also automated using Python and the Kinesis control software.

The sectioned samples can improve the understanding of bone marrow function as the cells have minimum damage, which is helpful in leukemia research.

**Keywords:** Laser microtomy, Femtosecond laser, Flat top profile, Beam shaping, Femur bone, Bone sectioning, Thermal shock zone

## REFERENCES

1. Lubatschowski, Holger. "Laser Microtomy: Opening a New Feasibility for Tissue Preparation." *Optik & Photonik*, vol. 2, no. 2, June 2007, pp. 49–51. DOI.org (Crossref), <https://doi.org/10.1002/opph.201190252>.
2. Will, Fabian, and Heiko Richter. "Laser-based Preparation of Biological Tissue: Femtosecond Lasers Speed up Histological Procedures in Medtech." *Laser Technik Journal*, vol. 12, no. 5, Nov. 2015, pp. 44–47. DOI.org (Crossref), <https://doi.org/10.1002/latj.201500036>.
3. Gemini, Laura, et al. "Ablation of Bone Tissue by Femtosecond Laser: A Path to High-Resolution Bone Surgery." *Materials*, vol. 14, no. 9, May 2021, p. 2429. DOI.org (Crossref), <https://doi.org/10.3390/ma14092429>.

**Title:** Evaporation Dynamics of Optically Levitated Droplets Smaller than 5 microns under Near-Infrared Heating.

**Presented By:** Jugal Rakesh Shah (*Bachelor's Student*)

**Authors:** Jugal Rakesh Shah<sup>1, 2</sup>, Javier Tello Marmolejo<sup>1</sup>, Max Huisman<sup>3</sup>, Devendra Deshmukh<sup>2</sup>, Dag Hanstorp<sup>1</sup>

**Affiliations:** <sup>1</sup> Department of Physics, University of Gothenburg, SE-412 96 Gothenburg, Sweden,

<sup>2</sup> Department of Mechanical Engineering, Indian Institute of Technology, Indore 452017, MP, India,

<sup>3</sup> SUPA and School of Physics and Astronomy, The University of Edinburgh, Peter Guthrie Tait Road, Edinburgh EH9 3FD, United Kingdom

**Abstract:** Evaporation dynamics of droplets are critical in atmospheric sciences, combustion, and industrial processes. In scenarios such as cloud formation and laser diagnostics of fuel droplets, radiative heating, including laser irradiation, significantly influences evaporation rates, often resulting in deviations from established theoretical models. Using optical levitation, we can suspend droplets in the air and study them under controlled heating. The classical  $D^2$ -law estimates droplet evaporation, assuming stable conditions and fast mixing. However, its accuracy is limited in laser diagnostics or cloud formation, especially for droplets smaller than 5 microns, like those in aerosols or fuel sprays. Studying these small droplets is difficult because they are hard to trap. Here we show how the single-component water droplets smaller than 5 microns evaporate under near-infrared heating. We find that the evaporation does not fully follow the  $D^2$ -law, showing a different pattern. As droplets shrink, their heat absorption changes, which likely causes these differences. Understanding these behaviors helps improve applications where droplet evaporation is important.

## Figures:

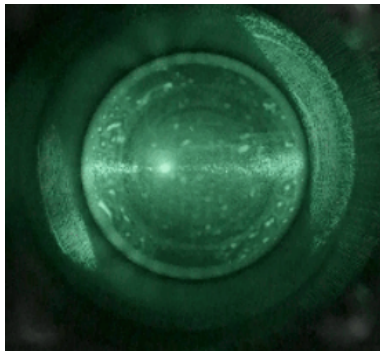


Fig. 1: Water droplet trapped in a counter-propagating optical trap.

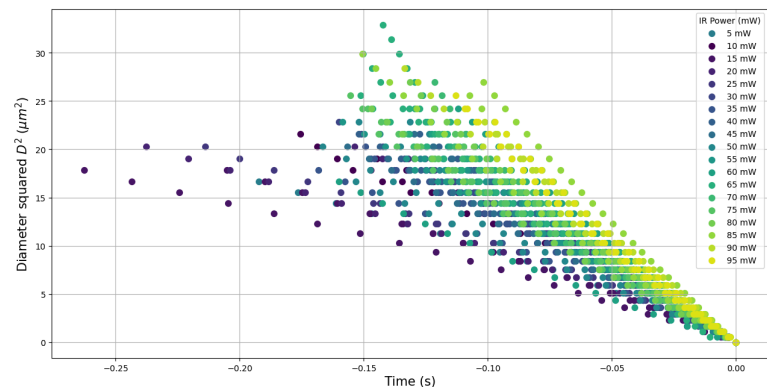


Fig. 2: Temporal Evolution of droplet diameter squared under different levels of NIR heating.

## References:

1. Javier Tello Marmolejo, Adriana Canales, Dag Hanstorp, and Ricardo Méndez-Fragoso, "Phys. Rev. Lett.," **130**, 043804 (2023).
2. G. Mie, "Ann. Phys.," **330**, 377-445 (1908).
3. S. Pokharel, A. Tropina, and M. Shneider, "Numerical modeling of laser heating and evaporation of a single droplet," *Energies*, vol. **16**, no. 1, 2023. [Online]. Available: <https://www.mdpi.com/1996-1073/16/1/388>
4. Leonid A. Dombrovsky, Alexander A. Fedorets, Vladimir Yu Levashov, Alexei P. Kryukov, Edward Bormashenko, and Michael Nosonovsky, "International Journal of Heat and Mass Transfer," **161**, 120255 (2020). ISSN 0017-9310.
5. F. Dalla Barba, J. Wang, and F. Picano, "Physics of Fluids," **33**(5), 051701 (2021).

# Comparison of layered coating materials in a neutral particle detector plate.

B. Ramírez<sup>1,2</sup>, D. Hanstorp<sup>2</sup>, R. Cabrera<sup>1</sup>, D. Leimbach<sup>1</sup>, and J. Snikeris<sup>1</sup>

<sup>1</sup>Department of Physics, University of Gothenburg, SE-412 96 Gothenburg, Sweden

<sup>2</sup>Facultad de Ciencias, Universidad Nacional Autónoma de México, Alcaldía Coyoacán

Negative ions have gained significant interest since they can explain the behaviour of a quantum system when the single particle model breaks down. These systems emerge when an electron binds to a neutral system that does not experience the long-range Coulomb force. This highlights the importance of the electron correlation and the interest in studying the electron affinities for numerous elements. The Gothenburg University Negative Ion Laser Laboratory (GUNILLA) has thoroughly analyzed these systems by using laser photodetachment threshold spectroscopy to study the p-wave electron in Tungsten ( $W^-$ ). A neutral particle detector with a graphene-based target is used to track neutral atoms resulting from the photodetachment process. The target must be a transparent plate to allow laser light to pass through while also serving as a conducting material to prevent it from becoming electrically charged, hence a glass or quartz plate coated with a conducting layer is the solution.

However, in recent analysis, the performance shown by the graphene layer on the detector's plate has degraded due to prolonged use, reducing the necessary conductivity for accurate measurements and contributing to unexpected results. Replacing the graphene-coated quartz plate with a material of similar properties such as an Indium Tin Oxide (ITO) plate is expected to improve the results in the spectroscopy, allowing the p-wave in Tungsten ( $W^-$ ) to be observed as it has been in previous papers. A comparative analysis using different plates in the detector will determinate whether the deterioration of the graphene layer was responsible for the observed changes. This might also provide some insight into how prolonged radiation exposure affects the coating materials in the neutral particle detector plate.

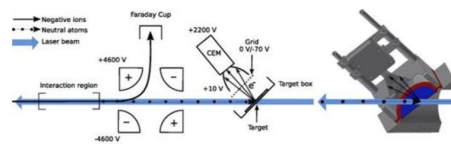


Figure 1: Schematic representation of the interaction region and the neutral particle detector. Right next to it, the CAD-model of the neutral particle detector used. [3]

## References

- [1] Lindahl, A., Andersson, P., Diehl, C., Forstner, O., Klason, P., Hanstorp, D. (s. f.). The electron affinity of tungsten. *The European Physical Journal D*, 60(2), 219-222. <https://doi.org/10.1140/epjd/e2010-00199-y>
- [2] Karls, J. (2021). Binding energies and lifetimes in negative ions [PH.D. THESIS]. University of Gothenburg.
- [3] Warbinek, J., Leimbach, D., Lu, D., Wendt, K., Pegg, D. J., Yurgens, A., Hanstorp, D., Welander, J. (2019). A graphene-based neutral particle detector. *Applied Physics Letters*, 114(6). <https://doi.org/10.1063/1.5080517>

# Interferometric quantum control (IQC) by fs/ns rotational coherent anti-Stokes Raman spectroscopy (RCARS)

M. Raveesh<sup>1</sup>, A. Dominguez<sup>1</sup>, M. Linne<sup>2</sup>, J. Bood<sup>1</sup> and A. Hosseinnia<sup>1</sup>

<sup>1</sup>Div. of Combustion Physics, Dep. of Physics, Lund University, Box 118, 221 00 Lund, Sweden

<sup>2</sup>Chair of Optical Diagnostics in Energy, Process and Chemical Engineering, RWTH-Aachen University, Schinkelstrasse 8, 52062 Aachen, Germany

<sup>3</sup>School of Engineering, The University of Edinburgh, Edinburgh EH8 3JL, Scotland  
[meena.raveesh@fysik.lu.se](mailto:meena.raveesh@fysik.lu.se)

Coherent Anti-Stokes Raman Spectroscopy (CARS) considered a gold standard for thermometry in reactive flows. We introduce a novel method to further enhance its diagnostic capabilities using quantum control by engineering the interference of two quantum wavepackets. This involves a 2-beam [1] hybrid fs/ns rotational CARS [2] setup with a second control pulse having a variable delay. The initial femtosecond (fs) pulse creates a rotational wavepacket. When the control pulse arrives at an integer multiple of the molecular revival period ( $T_{rev}$ ) it generates a wavepacket in phase with the initial one, leading to constructive interference and signal amplification. This is especially beneficial in high-temperature applications with low species number density. Conversely, if the control pulse arrives at an integer multiple of half the revival period ( $\frac{1}{2} T_{rev}$ ), it creates an out-of-phase wavepacket, resulting in destructive interference and signal annihilation. This allows for improved species-specific detection by eliminating specific molecular fingerprints in complex mixtures. By selecting an optimal delay time, we can enhance species selectivity and measurement accuracy in real-time, non-stationary reactive flows. Figure 1 shows the theoretical and experimental spectro-temporal map of IQC-RCARS with variable delay, demonstrating the efficacy of this approach.

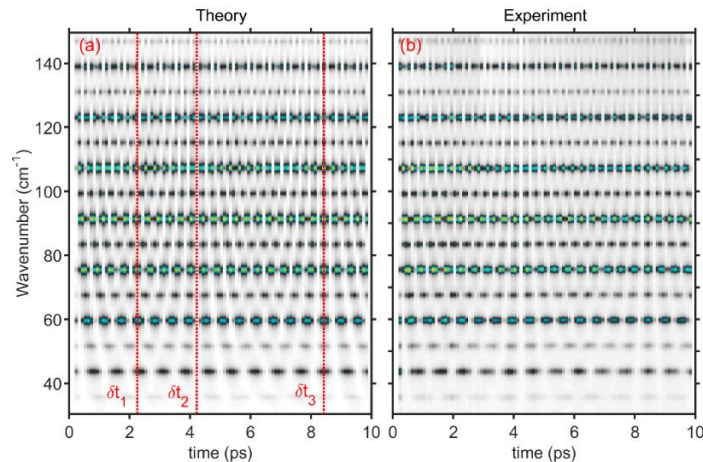


Figure : (a) Theoretically prepared spectro-temporal mapping of IQC-RCARS spectra with respect to pump-control pulse delay ( $\delta t$ ), by a step of 100 fs and (b) corresponding experimental data. The red vertical dashed lines indicate special spectra at  $\delta t_1 \approx 2.01$  ps ( $1/4 T_{rev}$ ) for selective nuclear-spin-isomer excitation,  $\delta t_2 = 4.19$  ps ( $1/2 T_{rev}$ ) for species-selective signal annihilation, and  $\delta t_3 = 8.38$  ps ( $T_{rev}$ ) for species-selective signal amplification.

1 A. Bohlin, B D. Patterson, and C J. Klierer, *The Journal of chemical physics* 138.8 (2013): 081102.

2 A. Hosseinnia, M. Ruchkina, P. Ding, P.-E. Bengtsson, and J. Bood, *Optics Letters*, 45 (2020) 308-311.

3 M. Raveesh, A. Dominguez, M. Linne, J. Bood and A. Hosseinnia, *Optics Express* 31, 38064-38076 (2023)



## Optimizing magnetic traps for diamagnetic particles

E. Rodríguez, J. Shah, K. Volke, D. Hanstorp, J. Marmolejo

Given that optical and electrostatic traps present problems like electrodynamic noise or particle damage, magnetic traps have emerged as a viable alternative. These traps use powerful magnets to create a small zero-field point between them, surrounded by strong magnetic field gradients. Diamagnetic particles are repelled by magnetic field and become trapped in the zero-field point. Despite the promising potential, there is insufficient information about the limits of magnetic traps for micro-sized particles. Here we show the progress towards characterizing a magnetic trap for water and silica particles. Optimizing parameters such as the separation distance between the tips ( $d$ ) and the angle of the magnetic tips ( $\theta$ ), we will be able to determine the maximum size of particles that can be stably trapped and their trap stiffness ( $k$ ).

This provides a cheap and safe alternative to study micro-particles without high laser power. Additionally, since we expect the vertical stability position depend on the mass, we foresee the possibility of measuring the weight of micro particles through their vertical displacement.



Fig 1. Water droplet trapped between two neodymium magnetic tips illuminated by a 532 nm low-power laser.

## References

1. O'Brien, M., Dunn, S., Downes, J., & Twamley, J. (2019). Magneto-mechanical trapping of micro-diamonds at low pressures. *Applied Physics Letters*, 114(5), 053103.
2. Gunawan, O., Kristiano, J., & Kwee, H. (2020). Magnetic-tip trap system. *Phys. Rev. Res.*, 2, 013359.
3. Lewandowski, C. W., Babbitt, W. R., & D'Urso, B. (2019, September). Comparison of magneto-gravitational and optical trapping for levitated optomechanics. In *Optical Trapping and Optical Micromanipulation XVI* (Vol. 11083, pp. 67-77). SPIE.

# Flat and miniature plasmonic biosensor enabled by metagrating-integrated vertical-cavity surface-emitting lasers

Erik Strandberg (1), Mindaugas Juodėnas (2), Hana Šípová-Jungová (3), Mikael Käll (3)

1: Chalmers University of Technology, Kemivägen 9, 412 58 Göteborg, erik.strandberg@chalmers.se

2: Kaunas University of Technology, 3: Chalmers University of Technology

## Abstract:

Driven by the increasing need for sensitive, rapid, affordable, and ease-of-use biosensors for medical diagnostics and biological research, an enormous amount of biosensing techniques and their corresponding devices have been developed in the last decades. In the plethora of biosensors, optical sensors based on the excitation of surface plasmon-polaritons, called surface plasmon resonance (SPR) sensors, have since their inception been one of the fastest-developing label-free sensing techniques [1]. Since the momentum of the surface plasmon lies beyond the light cone in air, the traditional SPR sensor uses a coupling prism to excite a surface plasmon in a thin metal film [2]. The prism limits the prospect of a miniaturized SPR-sensor which has kept the technique as a tool mainly used for research and in large bioindustry labs.

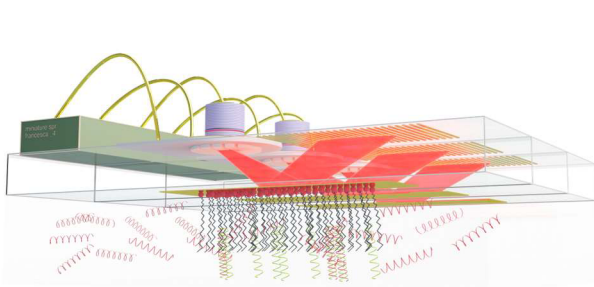


Fig. 1 3D-render of the full miniaturized SPR-sensor.

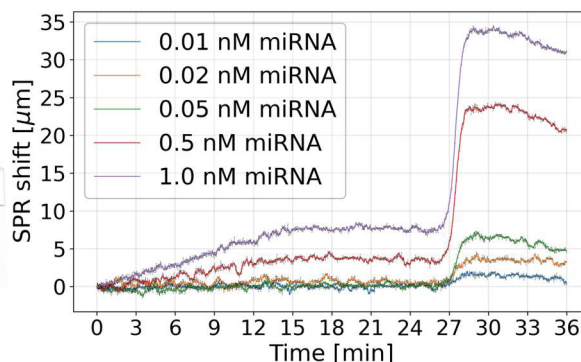


Fig. 2 Time trace from direct detection and antibody-amplified detection of miRNA.

We present a flat and miniaturized illumination module for SPR sensing, enabled by a vertical-cavity surface-emitting laser with a monolithically integrated metasurface [3]. The metasurface laser is bonded to a glass substrate and emits a beam into the glass that can be used for angle-resolved SPR sensing. On the opposite side of the surface plasmon supporting film, we have designed a simple multichannel microfluidic cell to flow different analytes to the sensor. We have characterized the device's performance, and we show that the resolution is comparable to the state-of-the-art at  $10^{-6}$  refractive index units [4]. We also demonstrate specific detection of microribonucleic acids (miRNA) for concentrations as low as 0.1 nM and 0.02 nM for direct detection and antibody-amplified detection, respectively [5]. We believe that this flat, highly scalable, and potentially affordable illumination source can pave the way for bringing SPR-sensing out of the lab and to be used for point-of-care devices.

## References

- 1 B. Liedberg, et al. "Surface plasmon resonance for gas detection and biosensing" *Sensors and Actuators*, vol. 4, 1983
- 2 J. Homola, "Surface plasmon resonance sensors for detection of chemical and biological species" *Chem. Rev.* vol. 2, 2008
- 3 M. Juodėnas, et al. "High-angle deflection of metagrating-integrated laser emission for high-contrast microscopy" *Light Sci Appl.* Vol 12, 2023
- 4 M. Piliarik, et al. "Surface plasmon resonance (SPR) sensors: approaching their limits?" *Opt Express*, vol. 17, 2009
- 5 Hana Šípová, et al. "Surface Plasmon Resonance Biosensor for Rapid Label-Free Detection of Microribonucleic Acid at Subfemtomole Level" *Anal. Chem.*, vol. 82, 20 10

## Determine higher-order dispersion constants in arbitrarily patterned waveguides

Albin J. Svärdsby and Philippe Tassin

Chalmers University of Technology, Department of Physics, SE-41296, Göteborg, Sweden  
albin.svardby@chalmers.se

**Abstract** – We report on our work on developing techniques to simulate long waveguides in nonlinear optics, taking the Kerr effect into account, with the use of the nonlinear Schrödinger equation (NLSE). To solve this equation, we need to determine higher-order dispersion constants. We show techniques to numerically calculate higher-order dispersion coefficients for arbitrarily patterned waveguides using eigenmode simulations using the finite-element method.

The nonlinear optical coefficients are very small for most materials. This results in a need for very long waveguides in integrated optics in order to achieve nonlinear optical processes such as optical parametric oscillation with appreciable efficiency, meter-long waveguide structures not being uncommon. This in turn makes simulations of nonlinear integrated optical devices challenging. Translationally invariant waveguides can be simulated using approximate methods such as the beam envelope method. However, for more complicated structures, for instance a periodically patterned waveguide, these approaches become unfeasible. In this contribution, we describe how the nonlinear wave propagation in periodically patterned waveguides with a  $\chi^{(3)}$  nonlinearity can be simulated using the nonlinear Schrödinger equation. We show how the weak form of Maxwell's equations can be rewritten in order to solve for propagation constants at fixed frequencies using eigenmode simulations in COMSOL. With this information, we can then determine the higher-order dispersion coefficients needed to solve the nonlinear Schrödinger equation for long, periodically patterned structures.

### ACKNOWLEDGEMENT

We acknowledge support from Chalmers' Excellence Initiative Nano and the Swedish Research Council. Some of the numerical calculations were performed on resources provided by the Swedish National Infrastructure for Computing (SNIC) at C3SE, partially funded by the Swedish Research Council.

# High-repetition-rate ultrafast light sources for attosecond science at the Lund Laser Centre

Ivan Sytceвич<sup>1\*</sup>, Ann-Kathrin Raab<sup>1</sup>, Chen Guo<sup>1</sup>, Anne-Lise Viotti<sup>1</sup>, Dominik Hoff<sup>1</sup>, Sara Mikaelsson<sup>1</sup>, Jan Vogelsang<sup>1,2</sup>, Mathieu Gisselbrecht<sup>1</sup>, Anders Mikkelsen<sup>1</sup>, Anne L’Huillier<sup>1</sup>, and Cord L. Arnold.<sup>1</sup>

<sup>1</sup>Department of Physics, Lund University, P.O. Box 118, SE-221 00 Lund, Sweden

<sup>2</sup>Institut für Physik, Universität Oldenburg, 26111 Oldenburg, Germany

**Abstract** We present an overview of an experimental infrastructure for attosecond science operating at 200 kHz repetition rate. Three light sources that deliver  $\mu\text{J}$ -level pulses with durations ranging from 6 to 31 fs in the near-(NIR) and short-wave infrared (SWIR), combined with high-order harmonic generation (HHG) in a high-pressure gas jet constitute an ideal platform for statistics-demanding studies in gases and solids.

In this work, we present a beamline for generation of attosecond pulses at 200 kHz repetition rate, involving three different laser sources for driving the HHG process. The layout of the experimental setup is shown in Fig. 1(a). All three laser branches are derived from the same Ti:Sapphire oscillator. Part of the oscillator spectrum around 1030 nm seeds an Ytterbium (Yb) chirped pulse amplification (CPA) chain, which serves as a pump for each of the outputs.

The workhorse of the beamline is an NIR optical parametric chirped pulse amplifier (OPCPA) [1]. Seeded by the rest of the oscillator spectrum, the amplifier emits 6 fs (2.2 cycle), carrier-envelope-phase (CEP) stable pulses at 850 nm with 15  $\mu\text{J}$  of energy. The output is focused into a high-pressure gas jet for HHG (a typical spectrum in argon is shown in Fig. 1 (b)), producing short trains of attosecond pulses in the extreme ultraviolet. This system is routinely used for studies of gas phase photoelectron dynamics using a 3D momentum spectrometer.

The second branch is based on nonlinear pulse post-compression of the Yb CPA laser in a multipass cell (MPC), using bulk glass as nonlinear medium [2]. This compression stage results in 150  $\mu\text{J}$ , 31 fs pulses at 1030 nm, allowing for the generation of <130 eV photon energies via HHG in neon (Fig 1 (c)).

The third branch is a recently developed SWIR OPCPA, producing CEP-stable, 2.3-cycle (16 fs), 13  $\mu\text{J}$  pulses around 2  $\mu\text{m}$ , capable of driving HHG in argon, Fig. 1 (d) [3].

Future development of the beamline involves an upgrade of the Yb pump laser, aiming to boost the output pulse energy of the two OPCPAs to hundreds of  $\mu\text{J}$ . This will allow for more energy-demanding attosecond XUV spec-

troscopy experiments with the NIR arm, and for the generation of water-window soft-X-Ray attosecond pulses from the SWIR arm. Furthermore, an additional compression stage for the MPC output is supposed to bring the pulse duration down to the few-cycle regime. Combined with CEP-tagging, this approach poses an attractive alternative to more experimentally complex, OPCPA-driven HHG platforms.

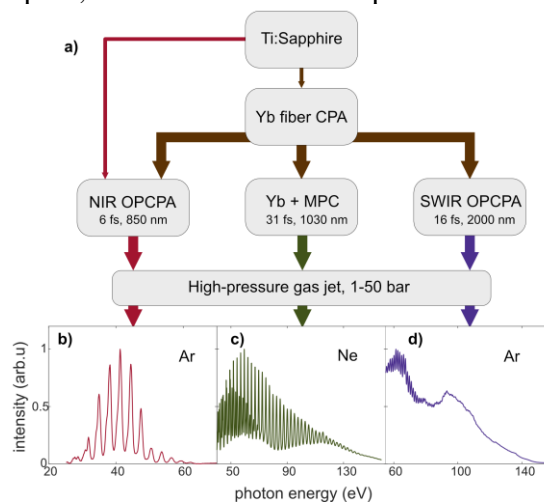


**Figure 1.** a) An illustration of the 200 kHz HHG beamline and typical HHG spectra for the output of: b) the NIR OPCPA (argon); c) the Yb MPC (neon); d) the SWIR OPCPA (argon).

## References

- [1] Mikaelsson S *et al* 2020 *Nanophotonics* **10** 117-128
- [2] Raab AK *et al* 2022 *Optics Letters* **47** 5084-5087
- [3] Sytceвич I *et al* 2022 *Optics Express* **30** 27858-27867

\* E-mail: [ivan.sytceвич@fysik.lth.se](mailto:ivan.sytceвич@fysik.lth.se)

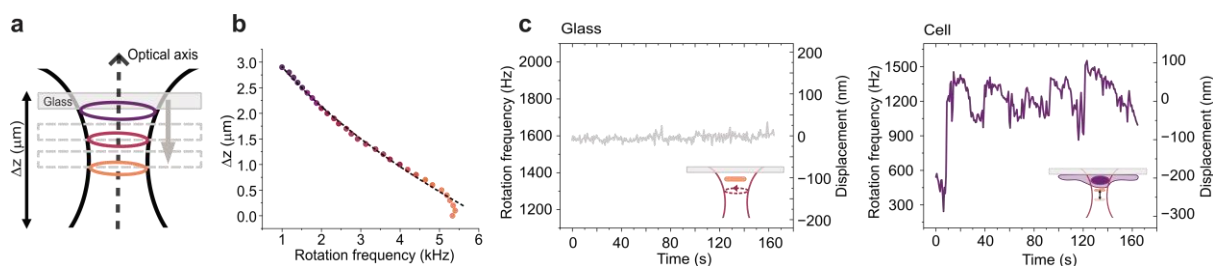
# Detecting Nanomotions of Single Cells using Optically Trapped Nanomotors

Authors:

Emelie Tornéus, Charlotte Hamngren Blomqvist, Caroline Beck Adiels and Hana Jungová

Understanding cells, the fundamental units of life, is crucial for advancements in fields like medicine and biotechnology. Advances in cellular research are closely linked to the development of methods that can measure nanoscale biological processes, both in time and space. A particularly important area is the study of mechanical motions in single cells, which are connected to cell viability and health<sup>1,2</sup>. To study these nanomotions, a highly sensitive, non-invasive method is essential.

We present a method for detecting nanomotions in living cells using a single rotating nanomotor trapped with optical tweezers<sup>3,4</sup>. Optical tweezers are a popular tool used in biological research due to their ability to sense and apply minute forces and torques to microscopic objects, as well as their ease of implementation allowing for precise studies of biological samples. In this approach, a nanorod supporting plasmonic resonances is trapped in two dimensions against a glass surface and rotated through torque transfer from a circularly polarized laser beam. The rotation frequency of the nanomotor is proportional to the optical torque, which is determined by the light intensity. By manipulating the nanomotor along the focus of the beam, this work demonstrates a near-linear relationship between its rotation frequency and position. Fluctuations of the cell membrane can displace the nanomotor along the laser beam, allowing for the detection of cellular nanomotions ranging from tens of nanometers to up to a micrometer. This opens new opportunities to study specific cellular processes, and in turn facilitating a deeper understanding of single-cell pathology.



Calibration curve acquisition for nanomotion detection by moving the microscope stage and measuring the rotation frequency at different positions along the laser beam axis. (a): Schematic representation. (b): Typical relationship between height offset and rotation frequency of a nanomotor (approximately  $164 \times 98 \text{ nm}$ ) at a laser power of  $5.5 \text{ mW}$ . The dashed line represents a fit with a second-order polynomial. (c) Rotation frequency and displacement in the z-direction over time for a nanomotor trapped over a glass surface (left) and over a cell (right).

## References:

- [1] Mojica-Benavides, M., van Niekerk, D. D., Mijalkov, M., Snoep, J. L., Mehlig, B., Volpe, G., Goksor, M. & Adiels, C. B. Intercellular communication induces glycolytic synchronization waves between individually oscillating cells. *Proceedings of the National Academy of Sciences* 118. issn: 0027-8424 (2021).
- [2] Venturelli, L., Kohler, A.-C., Stupar, P., Villalba, M. I., Kalauzi, A., Radotic, K., Bertacchi, M., Dinarelli, S., Girasole, M. & Pešić, M. A perspective view on the nanomotion detection of living organisms and its features. *Journal of Molecular Recognition* 33, e2849. issn: 0952-3499 (2020).
- [3] Shao, L., Yang, Z.-J., Andren, D., Johansson, P. & Kall, M. Gold nanorod rotary motors driven by resonant light scattering. *ACS nano* 9, 12542-12551. issn: 1936-0851 (2015).
- [4] Šipova, H., Shao, L., Odebo Lank, N., Andren, D. & Kall, M. Photothermal DNA-Release from Laser-Tweezed Individual Gold Nanomotors Driven by Photon Angular Momentum. *ACS Photonics* 5, 2168-2175 (2018).

## **Design, fabrication and characterization of advanced photonic devices for sensing applications**

Edoardo Trabaldo<sup>1</sup>, Olof Oberg<sup>1</sup>, Simon Watanabe<sup>1</sup>, Anatolii Makhinia<sup>1</sup>, Ingemar Petermann<sup>1</sup>, Yusuf Mulla<sup>1</sup> and Qin Wang<sup>1</sup>

Tom Yager<sup>2</sup>, Anete Berzina<sup>2</sup>, Boris Polyakov<sup>2</sup> and Anatolijs Sarakovskis<sup>2</sup>

<sup>1</sup>Research Institutes of Sweden (RISE), Sweden

<sup>2</sup>Institute of Solid-State Physics (ISSP), Riga, Latvia

Keywords: devices/sensors, nano/micro fabrications, printed electronics

Sensors are widely used in our daily life, and further development and improvement of current sensing technologies are continually demanded. They are driven by applications and markets in various areas including health, wellbeing, green energy, sustainable cities, as well as promotion of industry innovations.

In this work we present a few sensor examples, one is an integrated sensor utilizing graphene with asymmetric meta-surfaces to detect CO<sub>2</sub> and/or alcohol in IR regimes. Another is the development of THz detectors for sensing of illicit material for postal services and express courier flows within our ongoing EU project IFLOWS. It aims to enhance detection capabilities of dangerous and illicit goods transported within post and parcels flows in EU. The third example is the demonstration of printable photonic inks based on thermochromic ultra-fine VO<sub>2</sub> nanoparticles and hydrophobic Ag nanoparticles. This work was carried out successfully by joint effort from ISSP/RISE within EU Emerge project.